PROGRESS IN OPTICS

VOLUME XXXI

edited by **E. WOLF**, *Department of Physics and Astronomy, University of Rochester, NY, USA*

CONTENTS:

Previous volumes available:

Vol. XXX	1992	xix + 376 pages
Vol. XXIX	1991	xix + 438 pages
Vol. XXVIII	1990	xix + 438 pages
Vol. XXVII	1989	xx + 420 pages
Vol. XXVI	1988	xviii + 414 pages
Vol. XXV	1988	xvi + 448 pages
Vol. XXIV	1987	xviii + 532 pages
Vol. XXIII	1986	xvi + 294 pages
Vol. XXII	1985	xviii + 422 pages
Vol. XXI	1984	xvi + 446 pages
Vol. XX	1983	xvi + 400 pages
Vol. XIX	1981	xvi + 394 pages
Vol. XVIII	1980	xvi + 364 pages
Vol. XVII	1980	xvi + 362 pages
Vol. XIII	1979	xiv + 306 pages

ISBN 0-444-89836-9

WOLF PROGRESS IN OPTICS XXXI

EMIL WOLF

EDITOR

PROGRESS IN OPTICS

VOLUME XXXI

CONTRIBUTORS

G. DATTOLI
N.K. DUTTA
L. GIANNESSI
P.W. MILONNI
E. POPOV
D. PSALTIS
A. RENIERI
J.R. SIMPSON
R.J.C. SPREEUW
B. SUNDARAM
A. TORRE
J.P. WOERDMAN
Y. QIAO

PROGRESS IN OPTICS

VOLUME XXXI

EDITED BY

E. WOLF
University of Rochester, N.Y., U.S.A.

Contributors

G. DATTOLI, N. K. DUTTA, L. GIANNESSI, P. W. MILONNI, E. POPOV, D. PSALTIS, Y. QIAO, A. RENIERI, J. R. SIMPSON, R. J. C. SPREEUW, B. SUNDARAM, A. TORRE, J. P. WOERDMAN

1993

NORTH-HOLLAND
AMSTERDAM · LONDON · NEW YORK · TOKYO

CONTENTS

§ 1. Introduction

Diffraction gratings have attracted the attention of scientists for centuries, but they continue to exhibit such fascinating properties that the interest in them is still increasing. There are two primary reasons for gratings being used in several scientific disciplines. First, since they are used as a fundamental dispersive element, both manufacturers and users are vitally interested in the investigation and, if possible, optimization of grating properties. Moreover, the manufacturing process itself generates many problems for research into mechanics, lasers, optics, and materials (see, e.g., Hutley [1982], Loewen [1983]). Second, although simple in structure, gratings have proved to be so complex in behavior that the investigation of light diffraction by a periodically corrugated surface continues to be one of the most fascinating problems of the electromagnetic theory of light scattering. Throughout its development the theory has never been able to predict the entire spectrum of grating peculiarities, and as new phenomena (i.e. anomalies) appear that need further investigation, new theories arise. In addition, because of their structural simplicity, gratings are playing an important role as a model for other configurations, such as quasiperiodical and random rough surfaces (e.g., Maystre [1984b]).

1.1. GRATING ANOMALIES

Contrary to the nonscientist, the scientist is usually thrilled with the word "anomaly" – a paradox that is explained by the implication of something abnormal or unexpected, i.e., a new object for investigation. When Wood [1902] observed an unexpected property of diffraction gratings (i.e. a change in diffraction efficiency by a factor of more than 10 occurs in a spectral region not larger than the distance between sodium lines), he called that phenomenon "anomalous".

Each more or less rapid change in the diffraction efficiency of gratings is called an anomaly, even if it becomes a theoretically normal phenomenon. The great interest in the almost century-long investigation of anomalies has several explanations:

(1) Their appearance is connected to some physical phenomena that attract attention by themselves.

(2) Many anomalies result from surface wave excitations and could provide information on surface properties.

(3) Since it is more important to have a uniform rather than a high diffraction efficiency for most grating applications, anomalies must be avoided.

(4) In some cases high efficiency values could also be anomalous, and detailed investigations of anomalies could result in interesting applications.

(5) The theory of anomalies provides a valuable stimulus for the development of recent numerical methods for the analysis of the diffraction of light by relief gratings.

The first reviews on grating anomalies were published by Twersky [1956, 1960] and Millar [1961a,b]. More recently, Neviere [1980] and Maystre [1982] have contributed significantly to the physical understanding of anomalies and their classification. Although § 3 discusses in detail the present-day interpretation of different types of grating anomalies, some preliminary observations can be made. Three main types of anomalies can be distinguished:

(1) threshold phenomena that are connected with the energy distribution in propagating orders when some orders become evanescent;

(2) resonance anomalies that are due to the excitation of a guided wave along the corrugated surface (phase matching between the incident wave and a solution of the homogeneous problem are ensured by the grating); and

(3) nonresonance anomalies (sometimes called "broad" anomalies).

It is surprising that of the entire range of grating properties, almost nothing exists that has not been classified as an anomaly; as shown in § 2.2.1, even a completely regular type of behavior can be considered to be anomalous.

1.2. GRATING PROPERTIES AND PHYSICAL INTUITION

Over the past decade, many reviews and monographs have described the various theoretical, experimental, and technological problems and achievements of gratings (e.g., Petit [1980], Hutley [1982], Loewen [1983]). Today scientists believe and have proved that the electromagnetic theory of gratings based on the numerical implementation of the fundamental Maxwell's equations with appropriate boundary conditions can solve any problem involving light diffraction by periodic structures. Two "minor" difficulties, however, make this conclusion hypothetical rather than real, namely, numerical problems and cognition. The latter difficulty is typical for an understanding of

complex objects. Physical intuition is never satisfied simply by a knowledge of the basic facts; rather, understanding needs the determination of connections and analogies with something previously recognized and familiar. This idea was illustrated by Mermit [1990] using the example of recent quark theory: the knowledge of something being just an allowed combination of quarks contributes little to a real understanding of this entity. Similarly, sometimes a rigorous numerical modeling of the grating properties is insufficient to draw connections and analogies; calculations can stimulate, but not substitute for, thinking. A good example is the well-known property of metallic gratings to support two (the zeroth and first) diffraction orders in a Littrow mount, where the dispersive order propagates in a direction opposite to the incident wave: a quasiperiodicity in the diffraction efficiencies is observed as a function of the depth of the grooves. The theoretical explanation for this curious phenomenon, which is the focus of our interest here, could be found by starting from the simplest approaches based on Fresnel's principles, followed by scalar theories, and concluding successfully with recent electromagnetic methods. However, the further we go into more rigorous descriptions, the less helpful is physical intuition (see discussion by Petit and Cadilhac [1987]). For example, the simplest possible explanation is based on the following considerations: let us investigate a blazed (echelon) grating with a 90° apex angle (fig. 1) constructed from a perfectly conducting material, with light incident perpendicular to the larger facets. If the ratio of wavelength λ to the period d is properly chosen:

$$2 \sin \theta_0 = m(\lambda/d), \quad m = 0, \pm 1, \pm 2, \ldots, \tag{1}$$

the mth diffracted order propagates backwards towards the incident wave (fig. 1). If the angle of the grooves is equal to the angle of incidence θ_0, then a maximum efficiency could intuitively be expected for this mth order: light is incident normally on the large facet and is reflected backwards as if by a flat

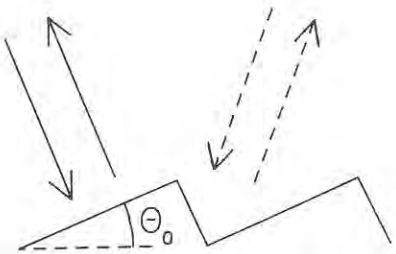

Fig. 1. Schematic representation of a blazed grating.

mirror. Equation (1) shows that the phase difference between rays reflected by two consecutive facets is equal to an integer times 2π; i.e., interference maxima appear in the far-field zone. According to eq. (1), such a maximum in the diffracted efficiency is repeated quasiperiodically with increasing m.
repeated quasiperiodically with increasing m.

Such a simple intuitive approach, however, could not explain why this phenomenon is independent of the sign of the angle of incidence (the dashed lines in fig. 1). If two diffraction orders are propagating, a perfect blazing in the Littrow mount can be observed when the incident wave is symmetrical with respect to the normal of the grating and is not perpendicular to any of the facets. Intuition fails completely when one realizes that this behavior in a Littrow mount is typical of the triangular and any other form of profile. Moreover, this quasiperiodicity (consecutive peaks and dips in the dependence of the efficiency on the groove depth) is common for other types of grating materials and incident conditions. This property is described in detail in § 2 for a variety of gratings. The results are obtained using rigorous electromagnetic methods. Most of these results have been confirmed experimentally.

Section 3 explains in phenomenological terms the phenomena that were introduced in § 2. Peculiarities in the efficiency are expressed using a small number of parameters (usually the poles and zeros of scattering matrix components), and their trajectories are followed when the groove depth is varied. These trajectories enable us to draw some unexpected new connections between different phenomena, such as surface wave excitation, Littrow and non-Littrow perfect blazing, and resonant and nonresonant total absorption of light. Section 3 also proves that the phenomenological parameters exhibit a quasiperiodical type of behavior. Thus it becomes obvious that the generality and importance of such behavior can be compared with the grating equation: whereas the latter guides the directions of the diffracted light, the quasiperiodicity determines the amount that is diffracted.

In § 4 a microscopic near-field picture is presented that enables us to visualize rigorous numerical results and to *see* what happens, to find out why it happens, and to determine why it is so general. In summary, it is shown that the behavior of reflection gratings is determined by the formation of regions with closed energy flow lines. Two main reasons explain why this physical interpretation (simple in its essence and illustrative in its presentation) of the numerical results was found only recently. First, it has not been clear where to look for a simple interpretation, since when dealing with the near-field zone, most scientists are interested in the energy power density and not in the energy flow direction. Second, theoretical and numerical difficulties prevent the possibility of obtaining the behavior of the electromagnetic field very close to the grating surface with sufficient precision, particularly for deep grooves, which is necessary because most phenomena are manifested only in deep gratings.

1.3. THEORETICAL APPROACHES TO GRATING PROPERTIES

As discussed in § 1.2, intuitive approaches not only failed to work even for the simplest configurations, but they also could not explain satisfactorily any of the grating anomalies, a topic of great interest since Wood's [1902] astonishing observation of the anomalous diffraction of light by a metallic grating. Lord Rayleigh [1907] was the first to realize that Fresnel's theory "tends to fail altogether when the (grating) interval is reduced so as to be comparable with the wave-length". His proposal for decomposition of the field into propagating and evanescent waves has provided a basis for the more recent approaches, although it includes diffracted orders that propagate only "upwards". By 1941 the Rayleigh method, as a precursor of recent electromagnetic theories, became commonly accepted (see Fano [1941]) as "following, in particular, work by Madden and Strong [1958] it becomes apparent that physical optics failed to give a satisfactory solution" (McClellan and Stroke [1966]).

Unfortunately, approaches based on the Rayleigh method cannot, in general, describe the field inside the grooves (except for shallow gratings, see Petit and Cadilhac [1966], Neviere and Cadilhac [1970], Millar [1971a,b], Van den Berg and Fokkema [1979]), although they could sometimes predict the far-field behavior (diffraction efficiencies) (Wirgin [1979a–c, 1980, 1981]). Van den Berg [1981] made an illustrative analysis investigating the convergence of the diffraction efficiencies and the satisfaction of the boundary conditions when the number of diffraction orders used in the calculations was increased; the convergence of the far-field results is not always accompanied by a fulfillment of the boundary conditions on the grating surface.

Differential methods are relatively simple to implement with computers (Petit [1966b], Neviere, Vincent and Petit [1974], Moaveni, Kalhor and Afrashteh [1975], Chang, Shan and Tamir [1980], Vincent [1980], Moharam and Gaylord [1982]), but they also exhibit convergence difficulties for highly conducting gratings when the magnetic field vector is parallel to the grooves (see Vincent [1980]). Thus, approaches must be used that are much more complicated and thus less attractive for programming, e.g., the integral method (Petit and Cadilhac [1964], Wirgin [1964, 1968], Uretsky [1965], Petit [1966a], Pavageau, Eido and Kobeisse [1967], Neureuther and Zaki [1969], Dumery

and Filippi [1970], Van den Berg [1971], Maystre [1972, 1973, 1978a,b, 1980]) or the conformal mapping approach (Neviere, Cadilhac and Petit [1972, 1973]). It is not our purpose to discuss in detail the nature, efficiency, and difficulties of different methods of light diffraction by periodic structures, but only to outline the main problems in the near-field investigations. Extended reviews on electromagnetic theory and its computer implementations can be found elsewhere (Petit [1980], Maystre [1984a]).

The importance of near-field results by themselves, and not only as a basis for the correct determination of efficiencies, concludes with a description of a brilliant example from a paper by Maystre [1984b]. A theory for electromagnetic scattering by a finite corrugated surface (figs. 2 and 3) is developed using the rigorous integral method of light diffraction by periodic structures. These impressive results warrant special attention: the distribution of electromagnetic field energy density in the near vicinity of a groove is almost equivalent to the corresponding distribution for an infinitely extending corrugation, provided the groove under investigation is separated from the surrounding plane region by several grooves. This phenomenon, called "short-coupling range", seems to have far-reaching, although not fully determined consequences. The first practical uses are in the theory of light diffracted by random rough surfaces that make it possible to reduce the computer memory storage and computation time

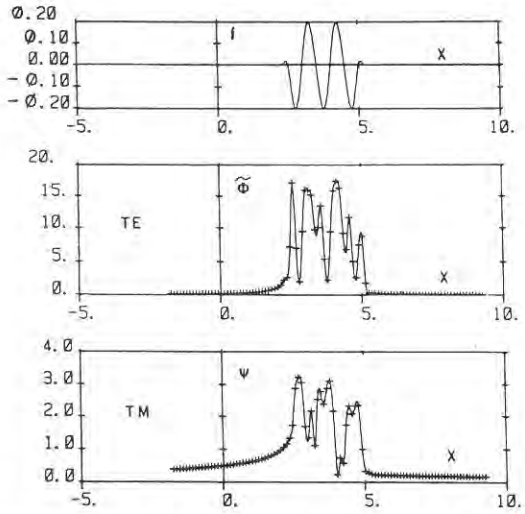

Fig. 2. The top part of the figure shows the shape of a finite grating with three grooves. The two other curves represent the difference between the actual surface current density and that corresponding to a perfect mirror: $\theta_0 = 30°$, $\lambda/d = 0.9$, $d = 1$, $h/d = 0.4$. (After Maystre [1984b].)

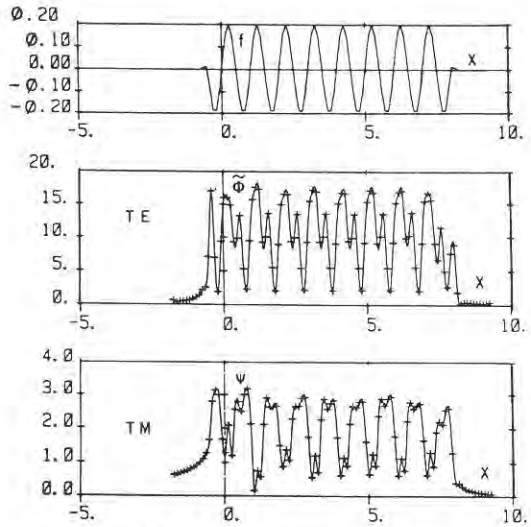

Fig. 3. The same as fig. 2, but with eight grooves. (After Maystre [1984b].)

significantly. Applied directly to the results given in § 4, the short-coupling range phenomenon permits us to conclude that, in general, these results are valid for structures with a limited number of grooves and, perhaps also, for rough surfaces.

§ 2. Quasiperiodicity: A Fundamental Property of Gratings

2.1. STATEMENT OF THE PROBLEM

Let us investigate a plane wave scattered by a periodic structure with a period d. The electromagnetic field $F(x, y)$ that is a solution of this problem is periodic to within a phase term,

$$F(x + d, y) = F(x, y) \exp[i(2\pi/d)x], \tag{2}$$

where F is any field characteristic and, in particular, its vector component along the grooves. We assume a classical diffraction case when an incident (and diffracted) wave vector is perpendicular to the grooves. We deal with a periodic corrugation (fig. 4) of the interface between two media that are characterized by their (complex) refractive indexes n_j, $j = 1, 2$. The upper medium is assumed to be lossless. The x-axis of the coordinate system introduced lies in the grating

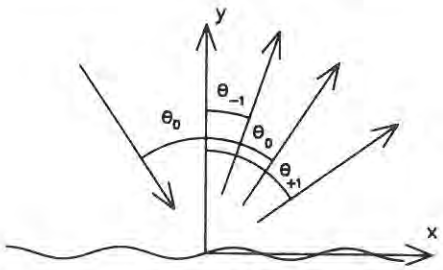

Fig. 4. Schematic representation of light diffraction by a grating.

plane and is perpendicular to the grooves. The z-axis is parallel to the grooves. Light is incident at an angle of θ_0 with respect to the y-axis. Two fundamental cases of polarization are identified that are mutually independent in the classical diffraction case (e.g., Petit [1980]). They are represented by the z-component of their electric ($\boldsymbol{E}$) or magnetic ($\boldsymbol{H}$) field vectors:

$$F(x, y) = \begin{cases} E_z, & \text{TE case}, \\ H_z, & \text{TM case}. \end{cases} \tag{3}$$

Due to the periodicity of the corrugations, incident light is diffracted into several orders with directions determined in the upper medium by the *grating equation*

$$\sin\theta_m = \sin\theta_0 + m(\lambda/d), \quad m = 0, \pm 1, \pm 2, \ldots . \tag{4}$$

If the second medium is also lossless, transmitted diffraction orders exist in directions determined by

$$n_2 \sin\theta_m^{(2)} = n_1 \sin\theta_0 + m(\lambda/d), \quad m = 0, \pm 1, \pm 2, \ldots . \tag{5}$$

Diffracted wave vectors are equal to $\boldsymbol{k}_m = k(\alpha_m, \chi_m, 0)$, where

$$\begin{aligned} k &= 2\pi/\lambda, \\ \alpha_m &= n_j \sin\theta_m^{(j)}, \quad j = 1, 2, \\ \chi_m^j &= (n_j^2 - \alpha_m^2)^{1/2}. \end{aligned} \tag{6}$$

If χ_m is real (for $m \in \mathbb{U}$), the corresponding order propagates away from the corrugated region, and if χ_m is imaginary, the order is evanescent. In the far-field zone defined by $|y| \to \infty$, the total field is a sum of the incident and

diffracted terms

$$F(x, y) = a_0 \exp[ik(\alpha_0 x - \chi_0 y)] + \sum_{m \in \mathbb{U}} b_m \exp[ik(\alpha_m x + \chi_m y)] \tag{7}$$

with amplitudes a_0 and $\{b_m\}$.

In general, the wavelength-to-period ratio determines the direction in which the light is diffracted (eqs. (4) and (5)). Another set of parameters, namely the groove profile $f(x)$, determines how much of the incident light is diffracted into those directions. For a fixed profile form the most general characteristic usually becomes the groove depth

$$h = \max_x[f(x)] - \min_x[f(x)]. \tag{8}$$

According to eq. (2), the total electromagnetic field is periodic along the x-axis parallel to the grating vector. Much more surprising is the existence of a quasiperiodicity in diffraction order amplitudes (their modulus and phases) as a function of groove depth h at other fixed parameters. It is impossible to predetermine this fundamental property from general considerations. It is investigated in this section for different grating periods, mountings, and materials.

2.2. REFLECTION GRATING SUPPORTING TWO DIFFRACTION ORDERS

2.2.1. *Littrow mount*

Two diffraction orders propagate in the first-order Littrow mount (when eq. (1) is satisfied for $m = -1$) when the wavelength-to-period ratio λ/d lies in the interval $(\frac{2}{3}, 2)$. Consecutive rises and falls of the diffraction efficiency with increasing groove depth are observed (fig. 5). This well-known type of behavior has been widely discussed. Although the behavior is regular, sometimes definite points in the groove depth dependence of the efficiency are considered to be anomalous: for decades the most unusual feature was thought to be the first specific region in fig. 5 with a zero efficiency in the specular order, accompanied by a maximum energy amount diffracted in the first order. This phenomenon is called "perfect blazing in a Littrow mount" (Roumiguieres, Maystre and Petit [1976], Breidne and Maystre [1980], Maystre, Cadilhac and Chandezon [1981], Maystre and Cadilhac [1981]), or "Bragg-type anomaly" (Tseng, Hessel and Oliner [1969], Hessel, Schmoys and Tseng [1975]). The primary reason for this interest is the practical importance of the maximum efficiency

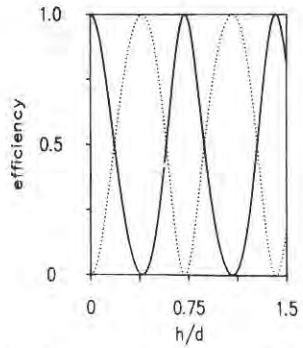

Fig. 5. Littrow mount efficiency as a function of groove depth of a sinusoidal perfectly conducting grating: $d = 0.5$ μm, $\lambda = 0.6238$ μm, TM polarization. The solid line represents the zeroth order and the dotted line represent the first order. (After Popov, Tsonev and Maystre [1990a].)

for the use of gratings. For metallic gratings the ratio of groove depth h_L to period corresponding to perfect blazing is approximately equal to $h_L/d \approx 0.40$ for TM polarization, being greater and strongly dependent on the wavelength for TE polarization (Petit [1980]).

For deeper grooves the first-order efficiency η_{-1} gradually decreases, and at some value of h, almost equal to two times h_L, η_{-1} becomes zero. The grating acts like a flat mirror throughout a large interval of angles of incidence (fig. 6): provided η_{-1} is zero in the Littrow mount, it is almost zero everywhere (independent on the mounting). This phenomenon is called the "antiblazing" of gratings, which is explained mathematically by energy conservation and symmetry considerations (Mashev, Popov and Maystre [1988]).

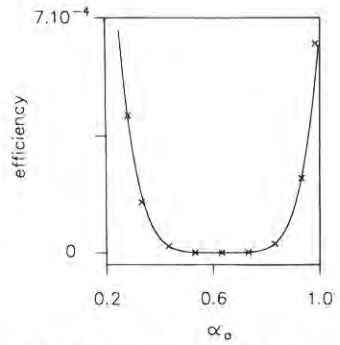

Fig. 6. Angular dependence of the first-order efficiency of a perfectly conducting sinusoidal grating, $d = 0.5$ μm, $\lambda = 0.6328$ μm, TM polarization, $\alpha_0 = \sin\theta_0$. (After Mashev, Popov and Maystre [1988].)

A further increase of the groove depth leads to a repetition of the behaviour of the efficiency; i.e., blazing is followed by antiblazing. A perfectly conducting substrate makes the blazing perfect, and all the incident energy is reflected back partially or totally into the zeroth or first order, their sum remaining equal to unity. For real metallic gratings in the visible region a similar quasiperiodic type of behavior is observed, the only difference being a slow reduction of the maximum efficiency values (Chandezon, Dupuis, Cornet and Maystre [1981]).

2.2.2. *Non-Littrow mount*

The quasiperiodicity of the efficiencies of highly reflecting gratings in the Littrow mount also appears for other incident angles. This can be expected in the light of the previously discussed antiblazing effect, since the first-order efficiency over a large angular interval becomes almost zero provided that it is zero in the Littrow mount (fig. 6). A typical example is presented in fig. 7; the efficiencies in the Littrow mount and in the grazing incidence exhibit similar quasiperiodic behavior. The maximum values in the grazing incidence are significantly lower than in the Littrow mount, but the positions of the minima coincide. In addition, fig. 7 presents results that contribute greatly to the generality of this type of behavior: the diffraction losses of a surface wave propagating along the same corrugated surface oscillate with the same period.

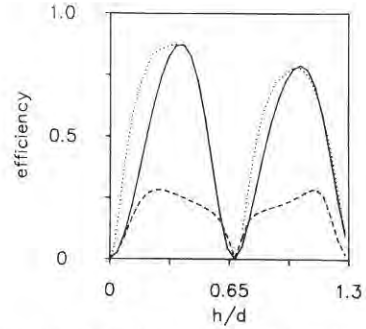

Fig. 7. Groove depth dependence of the efficiencies η_{-1} (the solid line represents the Littrow mount and the dashed line represents grazing incidence, with $\alpha_0 = 0.99$) and of the diffraction losses (dotted line) of a plasmon surface wave: $d = 0.5$ μm, $\lambda = 0.6328$ μm, TM polarization. (After Popov, Tsonev and Maystre [1990b].)

2.2.3. *Surface waves on corrugated metallic surfaces*

As mentioned in § 1.1, surface waves play an important role in grating anomalies. Their excitation leads to the formation of narrow dips and peaks in the diffraction efficiency (discussed in detail in § 2.3.2 and § 3.1). In this section the properties of the surface wave itself are analyzed.

Two diffraction orders propagate in the upper medium (air, with $n_1 = 1$) when

$$\lambda/d - 1 < |\sin\theta_0| < 1 . \tag{9}$$

In the case presented in fig. 7, $\lambda/d - 1 = 0.2656$. For angles of incidence characterized by $|\sin\theta_0| < 0.2656$, only the zeroth-order wave propagates; this case is examined in detail in the next subsection. The other limiting case, $|\sin\theta_0| > 1$, corresponds to surface wave propagation along the corrugated boundary. This surface wave has a propagation constant $k\alpha_S$ ($\equiv k \sin\theta_0$) and is characterized by an exponentially decreasing field with increasing distance from the interface. For a highly conducting metal–air boundary these waves are usually called plasmon–polariton surface waves (PSWs), which exist when the real part of dielectric permittivity of the metal is less than -1 (Neviere [1980], Maystre [1982]). The homogeneous problem (the existence of a nonzero scattered field without an incident field) on the plane surface has a solution with a propagation constant equal to

$$\alpha_S = \frac{1}{\sqrt{1 + n_2^2}} \tag{10}$$

and exists only for the TM polarization on a *bare* metallic surface.

When the media are lossy, even on a flat boundary the surface wave propagation constant becomes complex (eq. (10) with complex values of n_2). Its imaginary part $\mathrm{Im}\,\alpha_S$ corresponds to the absorption losses in the metal. For highly conducting metals the real part of α_S is slightly greater than unity. The surface corrugation has two simultaneous effects, resulting in the growth of $\mathrm{Im}\,\alpha_S$. First, it modifies slightly the absorption by the surface (fig. 8). By increasing the groove depth, the absorption losses grow proportionally to the average increase in the local-field density (Popov, Tsonev and Maystre [1990b]) rather than to the total area of the absorbing surface. This conclusion is further confirmed for deeper grooves: absorption losses exhibit consecutive rises and falls as a function of the groove depth (fig. 8b). Second, provided that the grating period is appropriately chosen to couple the surface wave to a

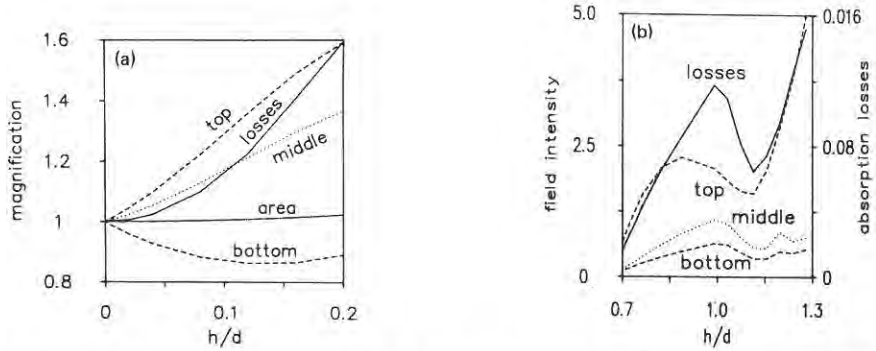

Fig. 8. Absorption losses of a plasmon surface wave as a function of groove depth (solid line) compared with the field intensity at the top, bottom, and in the middle of the grooves: $d = 0.5$ μm, $\lambda = 0.6328$ μm, TM polarization. (a) For a shallow grating, where the losses and intensities are given compared with their values on a flat surface. (b) deep grating, where the absolute values of the field intensity and absorption losses are given. (After Popov, Tsonev and Maystre [1990b].)

propagating order

$$-1 < \alpha_S - \lambda/d = \sin\theta_{-1} < 1 , \tag{11}$$

diffraction losses in the upper medium appear. The coupling between the surface wave and radiation order(s) depends on the groove depth for a fixed groove profile. For shallow gratings the coupling strength is proportional to h^2 (Reinisch and Neviere [1981]). For greater groove depth values, saturation is obtained (Chang and Tamir [1980]). If the groove depth is varied over much larger intervals than are commonly assumed in the research devoted to mode coupling, a quasiperiodic behavior can again be observed. It is surprising that the groove depth dependence of the diffraction losses precisely follows the efficiency behavior in the Littrow mount (fig. 7).

2.3. GRATING SUPPORTING A SINGLE DIFFRACTION ORDER

2.3.1. *Perfectly conducting grating*

We shall now examine the other case in eq. (9): if a plane wave is incident on the grating at an angle such that $|\sin\theta_0| < \lambda/d - 1$, only a single order propagates in the upper medium. In contrast to the case where a surface wave propagates (eq. (11)) this is the specular order that has a number $m = 0$.

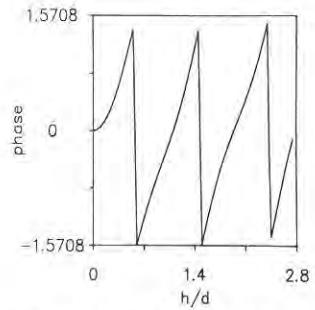

Fig. 9. Groove depth dependence of the phase of a wave reflected by a perfectly conducting sinusoidal grating: $d = 0.3$ μm, $\lambda = 0.6328$ μm, TM polarization, $\alpha_0 = 0.6328$. (After Popov, Tsonev and Maystre [1990a].)

Assuming perfect conductivity of the substrate, no variation of reflectivity can be expected due to the conservation of energy. Peculiarities can be found only in the phase of the reflected wave (fig. 9). It varies almost periodically when the groove depth increases by a large amount.

2.3.2. *Total absorption of light by metallic gratings*

In 1976 an unexpected theoretical discovery was made by Maystre and Petit [1976] that was verified experimentally by Hutley and Maystre [1976]. Whereas a flat mirror reflects almost all incident light, an only slightly corrugated surface under certain conditions can absorb it totally (fig. 10). These conditions include a set of angles of incidence, and wavelength and groove depth values, that are peculiar to a given substrate material and form of groove (fig. 10). During the following 15 years, this phenomenon (sometimes called Brewster's effect in metallic gratings) was investigated thoroughly. Its importance in grating studies can be compared with Wood's discovery of anomalous grating behavior. Its connection with the plasmon surface wave excitation was revealed and its resonant nature was proved (see § 3). We want to emphasize here that this phenomenon (total absorption of light, or TAL) is not an isolated case. It represents a manifestation for shallow gratings of a more general phenomenon (fig. 11). Investigations in a large groove depth interval indicate that repeating minima of reflectivity appear. A suitable choice of angle of incidence can diminish any reflection minima to a value of zero. It is remarkable that for an aluminum sinusoidal grating with red light ($\lambda = 0.6328$ μm), the three cases of total light absorption (for shallow, deep, and very deep grooves) almost coincide in position (fig. 11).

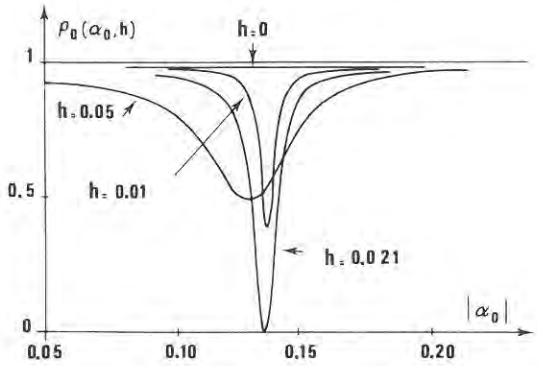

Fig. 10. Zeroth-order efficiency of a silver grating versus $\sin\theta_0$: TM polarization, $d = 1/2400$ mm, $\lambda = 0.5$ μm, given for different groove depth values, shown in the figure in microns. (After Maystre and Neviere [1977].)

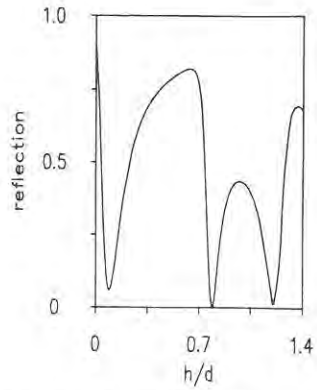

Fig. 11. Reflectivity (η_0) of an aluminum sinusoidal grating as a function of the groove depth: $d = 0.5$ μm, $\lambda = 0.6328$ μm, TM polarization, $\alpha_0 = 0.25762$. (After Mashev, Popov and Loewen [1989].)

The behavior of these anomalies when varying the entire set of system parameters will not be discussed in detail, but a few properties are worth noting. First, when a grating supports a higher number of orders, zeros in their amplitudes also exist, but these zeros are usually separated; they are manifested for different values of groove depth and angle of incidence (Maystre [1982]). The zeros of different orders can coincide only for highly specific sets of system parameters (§ 3.2, fig. 18). Second, resonance anomalies exist throughout the entire spectral region where the wavelength-to-period ratio is

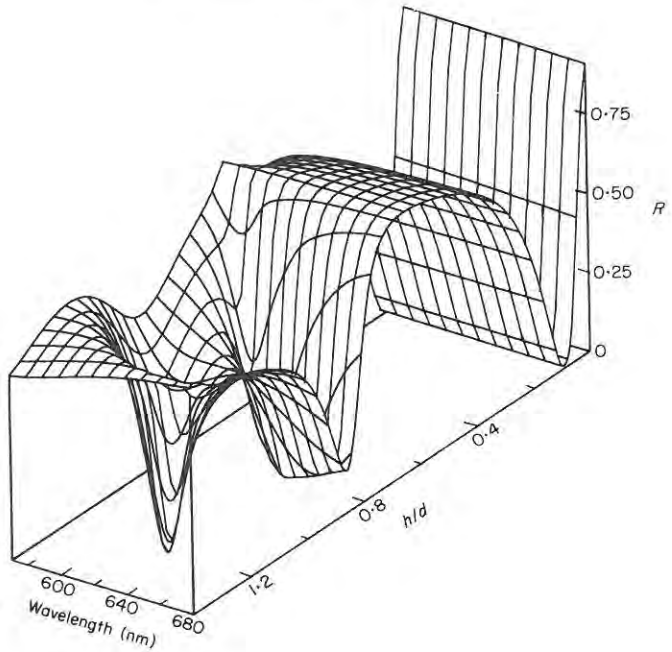

Fig. 12. Reflectivity of a sinusoidal aluminum grating as a function of the groove depth and wavelength: $d = 0.5$ μm, TM polarization. The angular deviation from the first-order cutoff is kept constant equal to 0.052°. (After Popov [1989].)

suitable for the excitation of surface waves. Because of the stronger coupling between surface waves propagating in opposite directions, the spectral behavior of anomalies in deep gratings is more complex than that for shallow grooves (fig. 12).

2.4. DIELECTRIC GRATINGS

The great interest devoted to perfect blazing in a Littrow mount derives primarily from its "blazing" properties, i.e., maximum diffraction efficiency in the dispersive order. It is usually assumed that the metallic substrate is a natural tool for obtaining high efficiency values. For some applications, however, even a small amount of energy absorbed by the substrate can be critical. These include the two limiting cases: either when very high light intensities can damage the grating material if absorbed even partially, or for very low intensities that are below the threshold of detection or laser generation.

It was proposed that a stack of layers on the corrugated metallic surface would increase the total reflectivity of the system (Maystre, Laude, Gacoin, Lepere and Priou [1980]). However, in contrast to dielectric multilayered flat mirrors, waveguide modes can be excited in grating structures that lead to multiple anomalies (Mashev and Popov [1984], Mashev and Loewen [1988]), thus limiting the application of these gratings.

In the 1980s two different mountings were proposed that make possible an almost perfect blazing by dielectric gratings. In the first mounting the idea of metallic gratings was suggested to reduce to a minimum the number of propagating orders using total internal reflection (TIR) (Popov, Mashev and Maystre [1988]). With light incident from the dielectric substrate side at an angle larger than the critical one for TIR, no diffracted waves are possible in air provided the period is small enough:

$$3\lambda > 2n_2 d \tag{12}$$

in the first-order Littrow mounting.

The groove depth dependence of the first-order efficiency is shown in fig. 13. Rises and falls similar to those of the efficiencies in metallic gratings are observed. An increase leads to a maximum of almost 100% followed by a minimum value of zero, etc. The two main differences in comparison with fig. 5 are that in the case of dielectric gratings, first, blazing occurs for a much greater groove depth-to-period ratio, and second, the maximum for TE polarization precedes the TM peak.

In the second case, when very high diffraction efficiency values are obtained,

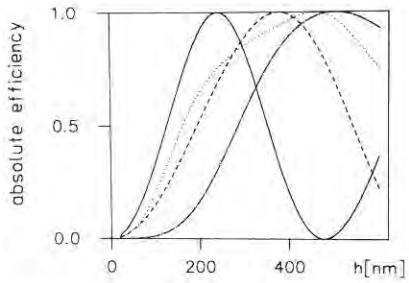

Fig. 13. Groove depth dependence of the efficiency of the first reflected order of a sinusoidal dielectric grating used from the substrate side in the Littrow mount: $n_1 = 1.5, n_2 = 1, d = 0.26$ μm. The solid line represents the TE polarization ($\lambda = 0.55$ μm), the dotted line represents the TM polarization ($\lambda = 0.55$ μm), the dashed line represents the TE polarization ($\lambda = 0.65$ μm), and the chain line represents the TM polarization ($\lambda = 0.65$ μm). (After Popov, Mashev and Maystre [1988].)

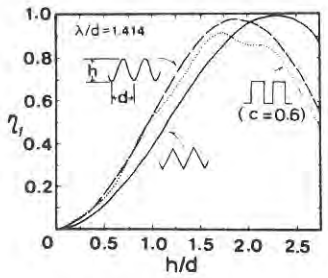

Fig. 14. Groove depth dependence of the efficiency of the first transmitted order for three different profiles. The light is incident from the substrate side: $n_1 = 1.66$, $n_2 = 1$, $d = 0.4476$ μm, $\lambda = 0.6328$ μm, TE polarization, $\theta_0 = 45°$. (After Yokomori [1984].)

a dielectric grating is used in a transmission regime in the so-called Bragg mounting, which requires the dispersion order to propagate symmetrically to the transmitted zeroth order with respect to the normal to the grating (Moharam and Gaylord [1982], Enger and Case [1983], Moharam, Gaylord, Sincerbox, Werlich and Yung [1984], Yokomori [1984]). The groove depth dependence of the efficiency is shown in fig. 14, and is similar to that presented in figs. 5 and 13. A quasiperiodicity is again observed, although its manifestation is now less obvious due to the larger groove depth values required for blazing and antiblazing.

§ 3. Phenomenological Approach: A Step Towards the Physical Interpretation of Grating Properties

By using a phenomenological approach to grating behavior, scientists expect to identify most variations and regularities in a small number of parameters. It is generally unnecessary, but strongly desirable for these parameters to have some physically obvious meaning. Nevertheless, it is satisfactory that the phenomenological approach may simplify some complex irregularity so that both the process and the results of simplification will bring us closer to an understanding of the investigated phenomenon.

Three investigative directions have been applied to the properties of the diffraction of light by periodically corrugated surfaces using a simplification (regularization) approach, each of which is a solution for a generally stated problem:

(1) What is the physical reason and interpretation of the narrow anomalies, best illustrated by the examples shown in figs. 10 to 12?

(2) Why do broad anomalies (i.e. regions of perfect blazing and antiblazing) exist, and what are their relationships with narrow anomalies?

(3) What is the physical background to the quasiperiodicity of the grating properties?

These three topics are discussed later in detail, but it is worth mentioning that in contrast with other physical problems, the phenomenological approach in grating theory is as rigorous as the recent numerical methods based on electromagnetic theory. This approach consists only of the proper choice of a larger number of regular parameters (believed to have a deeper physical meaning) rather than any simplification (approximation) of the theoretical methods. These phenomenological parameters can be determined with the same accuracy as any other quantity (e.g., phase, amplitude, efficiency). In fact, both sets are calculated using only slightly modified computer codes.

In this section we distinguish between resonance and nonresonance phenomena, calling them anomalies in the traditional way, although some demonstrate regular behavior. Generally, resonance anomalies are due to a surface wave excitation; a resonance between the incident wave and a solution of the homogeneous problem is ensured by the periodicity of the grating. Mathematically, this solution is expressed (discussed in detail in § 3.1) by a pole of the scattering matrix. Thus, as a working definition, it can be assumed that resonance anomalies are accompanied by a nearby pole, in contrast to the nonresonance ones. A preliminary observation should be made for clarification: resonance anomalies are usually narrow and nonresonance anomalies are broad, but there are some exceptions. Narrow dips in the angular and wavelength dependences of the efficiencies exist in the case of the almost total absorption of light by metallic gratings at grazing incidence (Mashev, Popov and Loewen [1988]), although this is a nonresonance anomaly. The half-width of minima and maxima in the reflectivity of corrugated waveguides due to waveguide mode excitation (resonance anomaly) depends strongly on the depth of the grooves (Popov, Mashev and Maystre [1986]) and can become sufficiently large. From a historical point of view, however, resonance anomalies sometimes are called narrow and nonresonance anomalies broad. That convention can safely be used only if the background reasons for specific anomalies are known.

3.1. RESONANCE ANOMALIES

Fano [1941] was the first researcher to draw a clear connection between narrow anomalies and surface wave excitation, distinguishing between "sharp"

and "broad" anomalies. Hessel and Oliner [1965] provided the following recently accepted formulation of a phenomenological approach to resonance (sharp) anomalies.

The surface wave propagation along a flat or corrugated surface is expressed mathematically by a solution of the homogeneous problem for light scattered by the surface without an incident wave. This solution requires the existence of a pole α^{P} of the scattering matrix $\boldsymbol{S}$ of the system, a pole that is equal to the surface wave complex propagation constant α_{S}. The scattering matrix determines the connection between the incident $\boldsymbol{a}$ and diffracted $\boldsymbol{b}$ wave amplitudes

$$\boldsymbol{b} = \boldsymbol{S}\boldsymbol{a} . \tag{13}$$

In fact, to have a nonzero solution for $\boldsymbol{b}$ without incident waves ($\boldsymbol{a} \equiv 0$), a zero of the determinant of the inverse of $\boldsymbol{S}$ is required. In the first-order approximation, $\det|\boldsymbol{S}^{-1}| \sim \alpha_0 - \alpha^{\mathrm{P}}$; i.e., each component of $\boldsymbol{S}$ is inversely proportional to $\alpha_0 - \alpha^{\mathrm{P}}$. Periodic corrugation multiplies the pole by the grating period (due to the coupling, the pole of one component of $\boldsymbol{S}$ becomes a pole of all the components):

$$\alpha_n^{\mathrm{P}} = \alpha_0^{\mathrm{P}} + n\lambda/d . \tag{14}$$

In particular, if a plane incident wave vector is phase matched to any homogeneous solution through eq. (14), the amplitude of any diffraction order (namely, the mth) should be proportional to

$$b_m \sim \frac{1}{\alpha_0 - \alpha_n^{\mathrm{P}}} . \tag{15}$$

For propagating orders (and, in particular, for the specular one) no anomalies occur without a corrugation. Thus, the pole is not manifested and has to be compensated by a zero α_m^z in the numerator such that $\alpha^z = \alpha^{\mathrm{P}}$ when $h = 0$. Corrugation removes the requirement for their equivalence, leading to a splitting, and the pole and the zero could be manifested in the amplitudes:

$$b_m \sim \frac{\alpha_0 - \alpha_m^z}{\alpha_0 - \alpha_n^{\mathrm{P}}} . \tag{16}$$

The different indexes in eqs. (15) and (16) have a different physical meaning. The index n of the pole corresponds to a surface wave excitation through the nth order. The amplitude (and the zero) index m represents the number of the order of interest.

Equation (16) represents the noted phenomenological formula that enables us to determine the behavior of the efficiencies in the region of a resonance anomaly (it is referred to as "resonance" due to the pole to which it has to be matched). Numerical results fully confirm the foregoing speculations that resulted in eq. (16). In general, pole and zero can be found for complex values of α_0, and their influence on the diffraction efficiency and the phase behavior can be satisfactorily traced for real angles of incidence following eq. (16). Its validity has been proved by a comparison of theoretical and experimental results (McPhedran and Maystre [1974], Maystre and Neviere [1977], Maystre, Neviere and Vincent [1978]). The coefficient of proportionality is a slowly varying function of the grating parameters. Pole and zero are independent of the angle of incidence and are slowly varying functions of groove depth and wavelength for a fixed form of groove profile. This characteristic is valid in the regions where the pole and zero are simple. When an anomaly interaction appears (e.g., when two surface waves are excited simultaneously), it can be expressed in the phenomenological formula by two (or more) terms with different poles and zeros corresponding to the excitation of separate surface waves.

For shallower gratings the splitting between the pole and the zero is smaller, in general, and the anomaly in the diffraction efficiency is sharper. For a perfectly conducting grating with a single propagating order, the energy balance criterion requires that the pole and the zero remain mutually complex conjugated. Let us remember that corrugation initiates diffraction losses of the surface wave, expressed in the growth of the imaginary part of the pole. Thus, the zero could also become complex. For real metallic substrates both the imaginary and real parts of the pole and the zero are slightly modified. Figure 15 presents their trajectories when the groove depth is varied, corresponding to the efficiency behavior seen in fig. 10. The position of α_0^z is almost symmetrical to α^{P} with respect to their initial position at $h = 0$. On increasing the corrugation depth, the trajectory of α_0^z crosses the real α_0 axis when $h = h_{\mathrm{B1}}$; a zero of the zeroth-order amplitude appears, which leads to the total absorption of incident light. For deeper grooves α_0^z moves away from the real axis and, according to eq. (16), the minimum value of the reflectivity increases (fig. 10).

A further increase of the groove depth leads to a stronger coupling between the surface wave and the order diffracted in the air. This phenomenon has two direct consequences. First, the diffraction losses increase (fig. 7), and the imaginary part of α^{P} rises (fig. 16). Second, above some critical value of groove depth, diffraction losses become so high that the surface wave is no longer localized at the surface; the real part of its propagation constant becomes less than unity. The pole is transferred into a zero of the zeroth-order amplitude, which is solitary, i.e., not accompanied by a pole (Popov, Mashev and Loewen [1989]).

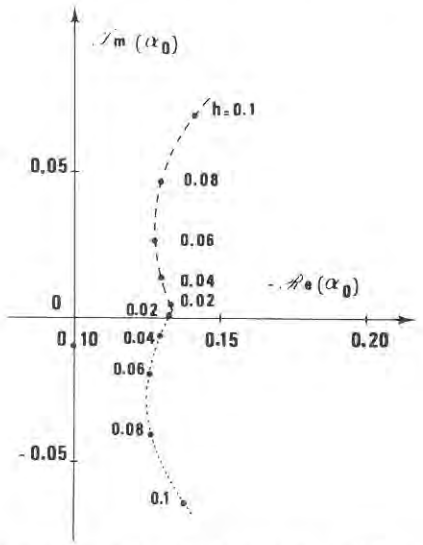

Fig. 15. Trajectories of the pole α^p (dashed line) and the zero of the zeroth reflected order α_0^z (dotted line) in the complex plane as a function of the modulation depth h/d, indicated with circles. The parameters of the sinusoidal silver grating correspond to those in fig. 10. (After Maystre and Neviere [1977].)

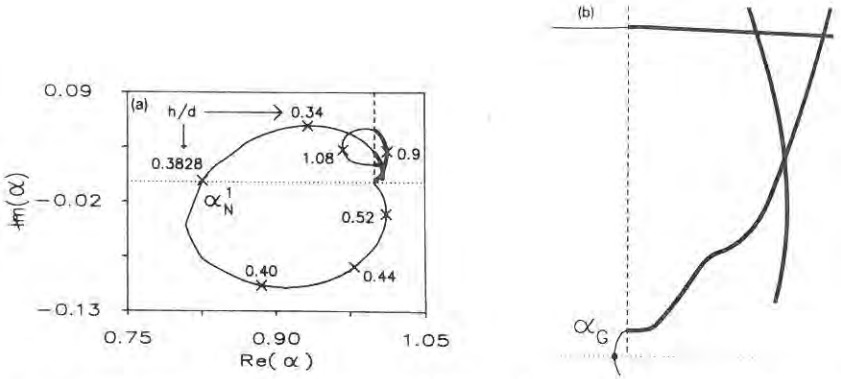

Fig. 16. (a) Trajectory of the pole α^p (heavy solid line) and zero α_0^z (thin solid line) in the complex plane when the groove depth is increased. The dotted line represents the real axis, and the dashed line represents the cut corresponding to the change of sign of χ_0. (b) Magnification (× 15) in the vicinity of point $\alpha_0 = (1, 0)$. (After Popov, Mashev and Loewen [1989].)

Following the trajectory of this newly born zero, the formation of loops is observed (fig. 16). Its cross-points with the real axis correspond with other anomalies that are not within the topic of this subsection, i.e., non-Littrow perfect blazing (α_N^1) and total absorption of light at grazing incidence (α_G) (see next subsection). When the trajectory again crosses the cut defined by $\mathrm{Re}(\alpha_0) = 1$, the zero becomes a pole, and a new branch of the plasmon surface wave propagation constant is obtained corresponding to the right-hand side of fig. 7. It is characterized by lower absorption losses than a surface wave on a flat surface (fig. 8b). An increase of the groove depth causes a new growth of the absorption and diffraction losses. Thus, a new loop is formed in the trajectory.

In fact, the position of the cut that starts from the point $\alpha_0 = (1, 0)$ is somewhat arbitrary (Maystre [1982], Mashev and Popov [1989]). The only restriction is that it lies in the upper half-plane. Nevertheless, this requirement is sufficient to distinguish between poles and zeros on the real α-axis, where the experimentally realizable angles of incidence are located. The meaning of the cut is to separate physical from nonphysical solutions, the first being defined by the proper radiation conditions at infinity (e.g., Petit [1980]). From that point of view all the zeros of the zeroth reflected order are indistinguishable and correspond to *one and the same* nonphysical solution of the homogeneous problem determined by the improper choice of the sign of χ_0 (Andrewartha, Fox and Wilson [1979a,b]). This conclusion has a practical application when dealing with the interaction between the different zeros, which behave like poles, demonstrating the splitting and repelling of trajectories (Mashev and Popov [1989]).

The pole tracing in fig. 16 corresponds to a surface wave carried through the zeroth order. As already mentioned, corrugation multiplies the poles: the fragments of the pole trajectory in fig. 17 correspond to a surface wave propagating to the left and excited through the first diffraction order. They are symmetrical with those in fig. 16 with respect to the position of the Littrow mount, and are accompanied by a zero (with trajectory starting from the point $\lambda/d - \alpha_S$ when $h = 0$). The trajectories of both pole and zero are piecewise continuous; they are divided by the cut that starts from the point $\alpha_0 = (\lambda/d - 1, 0)$.

As discussed in detail for fig. 10, the first cross-point α_B^1 with the real α_0-axis of the zero trajectory causes a total absorption of light by shallow gratings. The formation of loops in fig. 16 also results in the formation of loops in fig. 17. As a result, several cross-points of the trajectory of α_0^z with the real α_0-axis exist. The real zero α_N^2 that is situated in the region where two orders propagate is

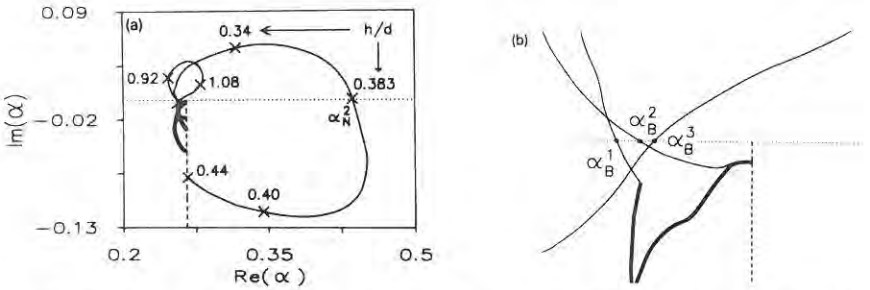

Fig. 17. Similar to fig. 16, but in the vicinity of the point $\alpha_0 = \lambda/d - 1$, corresponding to the beginning of the cut of χ_{-1}. (After Mashev, Popov and Loewen [1989].)

not accompanied by a pole, and it causes broad anomalies that are characterized by a minimum of the specular order efficiency and an increase of the first order. Thus, a non-Littrow perfect blazing (Maystre, Cadilhac and Chandezon [1981]) can be explained phenomenologically. The other two real zeros of the zero-order amplitude α_B^2 and α_B^3 lie below the first-order cut-off, and they describe the total absorption of incident light (the second and third minima in fig. 11).

3.2. NONRESONANCE ANOMALIES

In the preceding subsection we observed the existence of the zeroth-order zeros that are not accompanied by a pole. These are the perfect blazing in the non-Littrow mount and the "black hole" (Mashev, Popov and Loewen [1988]) at grazing incidence, expressed phenomenologically by the corresponding crossing points in figs. 16 and 17: α_N^1, α_N^2, and α_G. The presence of a pole can be registered by a substantial increase of the electromagnetic energy density in the near vicinity of the grating surface, as shown in § 4. Such poles and field enhancement do not occur for the nonresonance anomalies, although their behavior in the far-field region could be rather different; some (e.g., non-Littrow perfect blazing) are broad, whereas others are narrow (fig. 18). Moreover, the diffracted energy can vary from total absorption to perfect blazing. A simple explanation can be found in the relative independence of the specific behavior of the zeros of the different orders. That is, light absorption at grazing incidence occurs when simultaneous (but independent) zeros of the zeroth order (α_G) and first order (due to the antiblazing effect) exist for a specific value of groove depth (fig. 18), whereas blazing is characterized by a single zero of

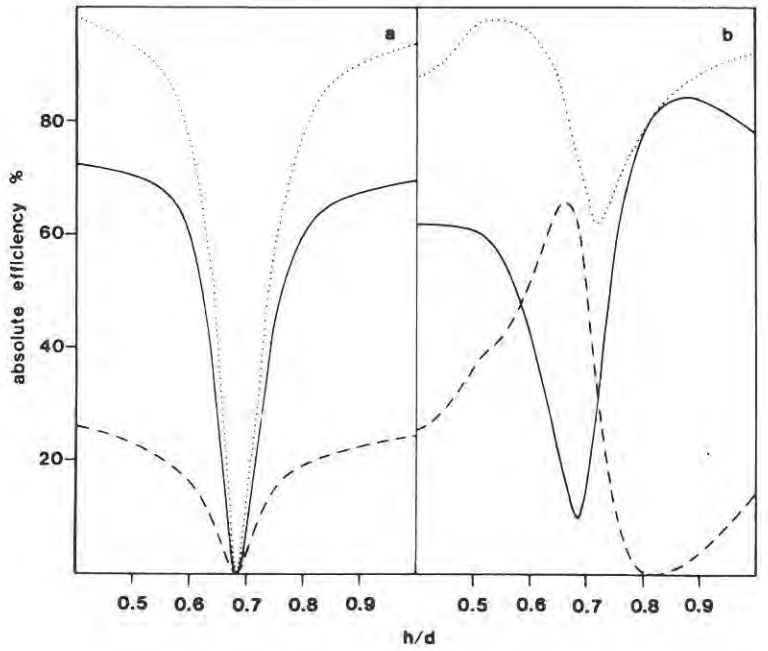

Fig. 18. Efficiency curves as a function of the modulation depth for an aluminum grating with $d = 0.50\ \mu m$, $\lambda = 0.6328\ \mu m$, $\theta_0 = 87.85°$, TM polarization. The solid curve represents the zeroth-order diffracted energy, the dashed line represents the first-order diffracted energy, and the dotted curve represents the total diffracted energy. (a) Sinusoidal groove profile, (b) symmetrical triangular groove profile. (After Mashev, Popov and Loewen [1988].)

the specular order, leading to a maximum of the first order. From that phenomenological point of view non-Littrow perfect blazing is equivalent to the perfect blazing in the Littrow mount, and both phenomena can be expressed by a zero of the specular order amplitude (without a nearby pole). They can be distinguished, however, by the origin of their trajectories when groove depth is varied. The non-Littrow perfect blazing and the light absorption at grazing incidence are connected (in a peculiar way) with the surface wave excitation along a flat interface in the groove depth regions, where such a wave is forbidden (fig. 16), whereas Littrow mount phenomena lie on a separate trajectory, as shown here.

Tseng, Hessel and Oliner [1969] were the first to notice that a Bragg-type anomaly is manifested by a zeroth-order real zero α_L^z. They distinguished between resonant and nonresonant anomalies, noticing that α_L^z has a specific type of behavior when varying the groove depth around its value h_L, which is responsible for perfect blazing in the Littrow mount; this zero moves along a

line perpendicular to the real α_0-axis. Their results were confirmed recently (Mashev and Popov [1989]) by following α_L^z over a large groove depth interval and, in particular, when $h \to 0$; the zero tends toward negative imaginary infinity along the line $\mathrm{Re}(\alpha_0) = \alpha_L^z$ defined by eq. (1). In contrast to the anomalies discussed previously, perfect blazing in the Littrow mount cannot be localized for flat surfaces. Whereas the other resonant or nonresonant phenomena can be specifically connected to a surface wave propagation along a flat interface, the zero α_L^z lies along a definitely separated trajectory (fig. 19), starting from $-i\infty$ for a flat surface. When the groove depth is increased, α_L^z moves towards the real axis, and the crossing point that appears for $h = h_{L1}$ leads to a maximum in the first-order efficiency, as shown in fig. 5. Increasing h, α_L^z goes away from the real axis, and the zeroth-order efficiency is proportional to $(\mathrm{Im}\,\alpha_L^z)^2$. Thus, the first-order efficiency decreases. At a groove depth value corresponding to the antiblazing effect, the zeroth-order zero α_L^z that is lying far in the upper complex α_0-half-plane is transformed into a second zero with a negative imaginary part (fig. 20). It results in a second perfect blazing in the Littrow mount for a further increase of groove depth.

If we return to the issues stated at the beginning of this section, the quasi-periodic character of the grating properties as a function of groove depth remains unclear. In fact, the phenomenological approach, which consists of expressing the grating peculiarities in terms of the poles and zeros and their tracing when the groove depth is varied, enables us to transfer these peculiarities into a specific behavior of the phenomenological parameters and to draw some interesting connections between the various grating properties. It remains unknown (and unclear from the intuitive point of view), however, why the

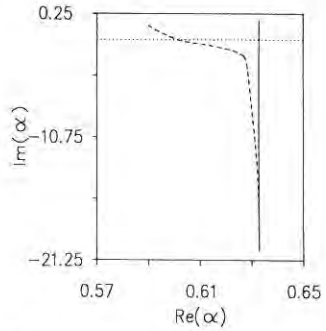

Fig. 19. Trajectory of α_L^z in a Littrow mount when the groove depth is varied: $d = 0.5$ μm, $\lambda = 0.6328$ μm. The solid line represents a perfectly conducting grating and the dashed line represents an aluminum grating. (After Mashev and Popov [1989].)

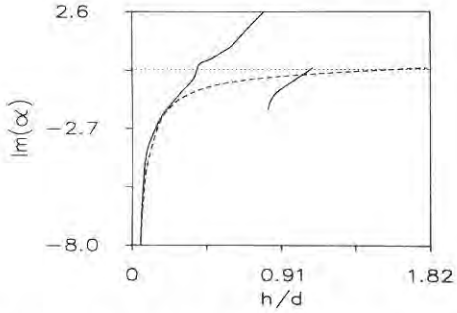

Fig. 20. Groove depth dependence of the imaginary part of the Littrow mount zero α_L^z, corresponding to the trajectory shown in fig. 19. The solid lines represents the TM polarization and the dashed line represents the TE polarization. (After Mashev and Popov [1989].)

Littrow mount zero of the zeroth-order amplitude exhibits some type of quasi-periodic behavior (fig. 20). An interesting attempt to introduce another set of phenomenological parameters was proposed by Maystre, Cadilhac and Chandezon [1981]. A detailed analysis of the properties of the scattering matrix makes it possible to show that in the Littrow mount the logarithmic eigenvalues $\pm\rho$ of the $\boldsymbol{S}$-matrix vary almost linearly with groove depth h (fig. 21) when only two diffraction orders propagate. A straight connection between ρ and η_{-1} leads to a periodicity in the groove depth dependence of the efficiencies:

$$\eta_{-1} = \sin^2\rho\,. \tag{17}$$

Although we believe that this approach has not received the acknowledgement it deserves, it has already proved useful. The possibility of perfect blazing in

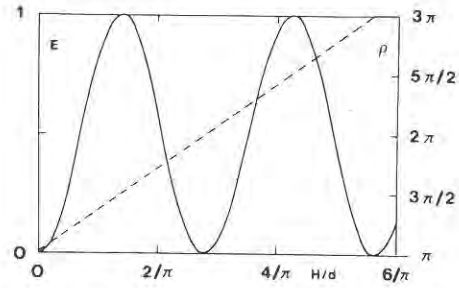

Fig. 21. Variation of the first-order efficiency (E) and of the phenomenological parameter ρ with the groove depth-to-period ratio for a sinusoidal grating with a wavelength-to-period ratio of $\lambda/d = 0.8$ for the TE case. (After Maystre, Cadilhac and Chandezon [1981].)

non-Littrow mounts was discovered as a result of a detailed study of the behavior of ρ.

§ 4. Microscopic Properties of Light Diffracted by Relief Gratings

The phenomenological parameters introduced in the previous section are shown to be precise tools for obtaining a more compact expression for the peculiar features of the gratings. Moreover, some of the physical reasons for these peculiarities could be found by simply tracing the behavior of the phenomenological parameters. A typical example is the total absorption of light in shallow gratings. The mechanism of its appearance becomes clear when one realizes why the existence of a zero in the propagation order amplitude is necessary to accompany the pole corresponding to a surface wave excitation.

It remains unknown, however, why the quasiperiodicity of the grating characteristics is such a general property. In fact, the phenomenological approach transfers the quasiperiodicity into loops in the trajectories of the poles and zeros (figs. 16, 17) or into the linearly varying parameter ρ (fig. 21), but it does not reveal why such loops are formed. These loops are not physical phenomena, but are a mathematical expression of the quasiperiodicity of the far-field properties. To find a physical explanation we have to go deeper into the physical process of diffraction of light by relief gratings. It should be pointed out that "deeper" does not mean more rigorous; as already discussed, even the phenomenological results may be sufficiently accurate; deeper is used in the sense of being more physical from the heuristic point of view. Such a physical explanation of quasiperiodicity can be found in the pictures of the distributions of energy flow lines. These lines are locally tangential to the Poynting vector $\boldsymbol{P}$, defined as

$$\boldsymbol{P} = \mathrm{Re}(\boldsymbol{E} \times \boldsymbol{H}^*)\,, \tag{18}$$

where the asterisk means complex conjugation. In some examples the local density of the electromagnetic field energy is also analyzed, where it has a peculiar behavior leading to specific phenomena of major importance, such as surface-enhanced Raman scattering (Reinisch and Neviere [1981], Metcalfe and Hester [1983], Yamashita and Tsuji [1983]), second harmonic generation (Neviere and Reinisch [1983], Reinisch, Chartier, Neviere, Hutley, Clauss, Galaup and Eloy [1983], Coutaz [1987], Neviere, Akhouayri, Vincent and Reinisch [1987], Maystre, Neviere, Reinisch and Coutaz [1988]), and surface plasmon luminescence (Coutaz and Reinisch [1985]).

Cases previously discussed are analyzed successively without classification into separate groups, since the properties they have in common are obvious.

4.1. PERFECTLY CONDUCTING GRATING IN LITTROW MOUNT

In the far-field zone the z-component of the electromagnetic field parallel to the grooves can be represented as a sum of incident, reflected, and diffracted orders. For TM polarization, when there are only two propagating diffracted orders in the Littrow mount, according to eqs. (3) and (7), this is the z-component of the magnetic field

$$H_z = a_0 \exp[\mathrm{i}k(\alpha_0 x - \chi_0^1 y)] + b_\mathrm{r} \exp[\mathrm{i}k(\alpha_0 x + \chi_0^1 y)] + b_\mathrm{d} \exp[-\mathrm{i}k(\alpha_0 x - \chi_0^1 y)]\,. \tag{19}$$

When the grating is reduced to a perfectly conducting plane mirror located on the x-axis, $b_d = 0$ and $b_r = a_0$.

Next, we assume that $a_0 \equiv 1$. Then it can easily be shown that for $h \neq 0$

$$P_x = \frac{k\alpha_0}{\omega\varepsilon_0 n_1^2}\,[|b_\mathrm{r}|^2 + \mathrm{Re}(b_\mathrm{r})\cos(2k\chi_0^1 y) - \mathrm{Im}(b_\mathrm{r})\sin(2k\chi_0^1 y)]\,, \tag{20a}$$

$$P_y = \frac{k\chi_0^1}{\omega\varepsilon_0 n_1^2}\,[\mathrm{Re}(b_\mathrm{r} b_\mathrm{d}^*)\cos(2k\alpha_0 x) - \mathrm{Im}(b_\mathrm{r} b_\mathrm{d}^*)\sin(2k\alpha_0 x)]\,, \tag{21a}$$

where $\omega = c/k$, c is the velocity of light in vacuum, and ε_0 is the vacuum permittivity. Equations (20a) and (21a) can be simplified more if we assume that the amplitudes b_r and b_d are real, which is almost true for shallow gratings. When the origin of the coordinate system lies on the corrugated surface, e.g., $f(x) = \frac{1}{2}h\sin(2\pi x/d)$, then

$$P_x = \frac{k\alpha_0}{\omega\varepsilon_0 n_1^2}\, b_\mathrm{r}[b_\mathrm{r} + \cos(2k\chi_0^1 y)]\,, \tag{20b}$$

$$P_y = \frac{k\chi_0^1}{\omega\varepsilon_0 n_1^2}\, b_\mathrm{r} b_\mathrm{d} \cos(2k\alpha_0 x)\,. \tag{21b}$$

4.1.1. *Flat surfaces*

In the familiar case of a flat mirror, the vertical (P_y) component of the Poynting vector becomes zero, as $b_\mathrm{d} = 0$. This case is characterized by flow

lines parallel to the surface (no losses occur in either medium). For TM polarization, P_x has a maximum on the surface ($y = 0$), and has a zero at heights given by

$$y_0^{\mathrm{TM}} = (2m + 1)\,\frac{\pi}{2k\chi_0^1}\,, \quad m = 0, 1, 2, \ldots . \tag{22a}$$

For TE polarization, P_x is zero at the surface and at heights given by

$$y_0^{\mathrm{TE}} = 2m\,\frac{\pi}{2k\chi_0^1}\,. \tag{22b}$$

P_x^{TE} has a maximum at the level where P_x^{TM} exhibits zeros.

4.1.2. *Shallow gratings*

When the groove depth is slightly greater than zero, the diffracted field amplitude also becomes nonzero. Since there is no absorption in either medium, in the very near vicinity of the grating the flow lines must follow the groove profile without osculating the surface (fig. 22a), and a curvature of the flow lines appears. In fact, eq. (21b) states that $P_y \not\equiv 0$, except for the vertical lines above the tops and bottoms of the grooves. The profile is defined by the equation $y = (h/2)\sin(2\pi x/d)$. Thus, in the Littrow mount ($2\alpha_0 = \lambda/d$), P_y becomes zero for $x = (2m + 1)d/2$, according to eq. (21b). Since now $|b_r| < 1$, each horizontal line at which $P_x = 0$ (eq. (20b)) is split into two lines (e.g., fig. 22b), the splitting increasing with the decrease of $|b_r|$, i.e. with the increase of groove depth. Between each two pairs of lines, P_x has an opposite sign compared with the case of the flat surface. The two dashed lines in fig. 22b correspond to the splitting of the dashed line in fig. 22a and represent the positions where P_x becomes zero. As a result of this changing of the directions of $\boldsymbol{P}$, so-called "curls" are formed around the points where $|\boldsymbol{P}| = 0$. It could easily be deduced that in lossless media $\mathrm{div}\,\boldsymbol{P} = 0$; thus, energy flow lines are either closed lines or end on the boundary of the medium. The regions with closed vector lines are called "curls", and they exist even for shallow gratings and are not typical only of light diffraction from a grating. When three waves are interfering, independently of their origin, regions where the curls exist occur throughout space, as can easily be shown from eqs. (20b) and (21b). These waves can result from the diffraction of light from a grating, and can also be radiated by three different coherent sources. Hajnal [1987] showed that the

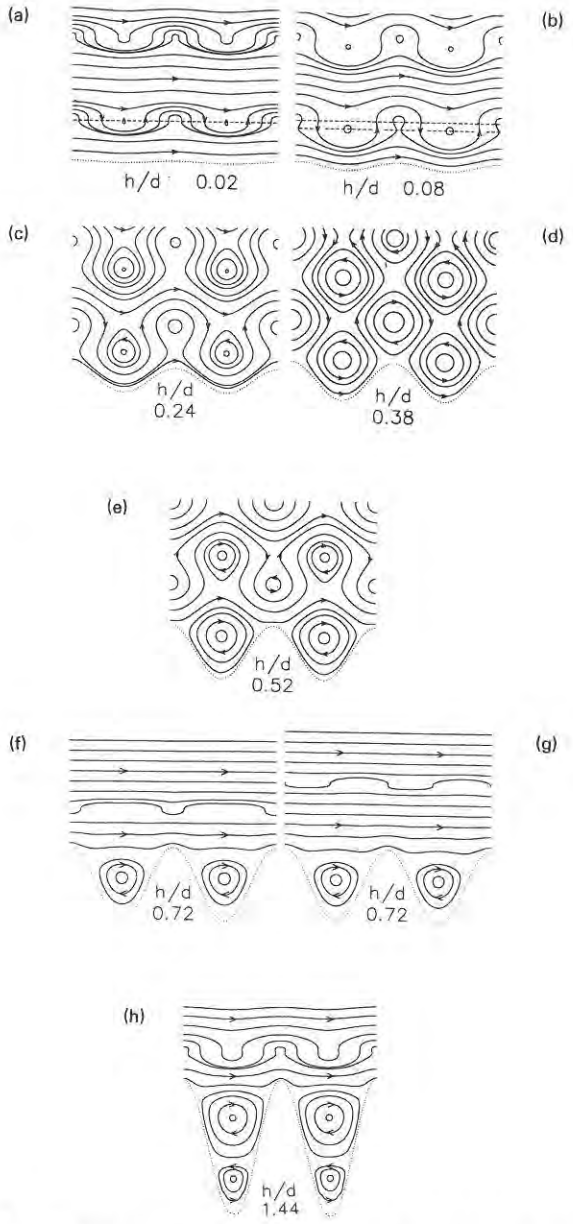

Fig. 22. Energy flow lines above a perfectly conducting sinusoidal grating. Littrow mount, $d = 0.5$ μm, $\lambda = 0.6328$ μm, TM polarization: (a) $h = 0.01$ μm, (b) $h = 0.04$ μm, (c) $h = 0.12$ μm, (d) $h = 0.19$ μm, (e) $h = 0.26$ μm, (f) $h = 0.36$ μm, (g) $h = 0.36$ μm and $\alpha_0 = 0.85$, (h) $h = 0.72$ μm. (After Popov, Tsonev and Maystre [1990a].)

interaction of three monochromatic circularly polarized electromagnetic waves can lead to highly interesting physical phenomena and field distributions.

Considering the grating again, we must point out that two different sets of curls can be found (fig. 22b), above the tops (labelled as "top curls") and above the bottoms (labelled as "bottom curls") of the grooves, the latter lying a little lower than the former. By increasing the depth of the grooves, the centers of the two sets of curls are shifted in the vertical direction, and the curls are enlarged, enveloping more and more flow lines. It is important to note that for TE polarization the formation of the lowest curls begins at a distance from the grating surface twice that for TM polarization, which is a direct consequence of eq. (22).

4.1.3. *Perfect blazing in Littrow mounts*

The increase in the size of curls means that increasingly few flow lines pass from left to right, i.e., less energy is carried towards the positive direction of the x-axis (fig. 22c). As a result, the amplitude of the reflected order b_r decreases, and an increase of the diffraction efficiency can be observed.

It is interesting to note that the centers of the lowest top curls and lowest bottom curls lie at an almost identical height from the grating surface. For this reason, when h grows, the vertical distance between the centers of the different sets of curls also increases almost proportionally to h. When the centers of the lowest bottom curls lie on the line connecting the tops of the grooves (fig. 22d), all the curls become uniformly distributed. The centers of the top curls are localized in the vertical direction exactly between the centers of the bottom curls. The curls then occupy the entire upper medium, and no energy flow towards $+x$ is observed, i.e., $b_r = 0$ and perfect blazing occurs. This happens, as can easily be predicted, when

$$h = y_0^{\mathrm{TM,\,TE}}. \tag{23}$$

When the evanescent waves are included in the near-field zone, eq. (23) becomes only an approximation, but a very good one. It must be pointed out that although the grating becomes increasingly deeper, the far- and near-field electromagnetic field distributions are identical, except for the groove area where the picture should depend strongly on the form of the profile.

Equations (22) and (23) explain why perfect TE blazing can usually be obtained at gratings almost twice as deep as those for the TM polarization: the lowest curls are formed at surfaces twice as high as those for the TM polarization, and groove depth values twice as high are required to bring the centers of the lowest bottom curls to the line connecting the tops.

When $b_r = 0$ it can easily be shown that not only all the flow lines are closed curves (fig. 22d) but also $|\boldsymbol{P}|$ vanishes everywhere in the upper medium. As h increases, the curls appear again, but they now rotate in the opposite direction. The bottom curls are lowered with h (fig. 22e). The increasing asymmetry in the position of the two sets of curls leads to a decrease of the area they occupy. Thus, more energy lines go from left to right, and b_r increases.

4.1.4. *Antiblazing of gratings*

The unfolding of the curls continues as the lowest bottom curls settle increasingly deeply in the grooves. The vertical distance between the centers of the second bottom curls and the first top curls decreases, and the actual energy flow distribution increasingly resembles the distribution of shallow gratings, except for the groove region. When the centers of both sets of curls lie on one horizontal line, the flow distribution above the grooves is the same as that above a plane surface. Then the first (i.e. the lowest) bottom curls completely separate the flow above the grooves from the groove surface (fig. 22f). Their deformation is such that they follow the profile.

Since the flow is the same as that above a flat surface, no diffraction is observed ($b_d = 0$). The curls inside the grooves are stable and feel little influence from the angle of incidence (fig. 22g with $\alpha_0 = 0.85$). In this way, antiblazing of gratings can be given a physical interpretation.

4.1.5. *Very deep gratings*

A further increase of h leads to a repetition of the flow distribution for shallow gratings, except for the existence of a hidden curl inside each groove. These curls become gradually lower inside the grooves as h increases. For very deep grooves a second perfect blazing appears ($h/d = 1.08$ in fig. 5), followed by a second antiblazing. The latter is characterized by two hidden curls inside each groove that separate the flow above the grooves from the bottom of the groove (fig. 22h).

4.2. PERFECTLY CONDUCTING GRATING SUPPORTING A SINGLE DIFFRACTION ORDER

The energy flow distribution above a perfectly conducting grating, which supports only a single diffraction order, has a similar behavior. As shown in § 2.3.1, a quasiperiodicity of the phase of the reflected wave can now be observed (fig. 9) in the far-field zone. In the near-field zone the formation of curls can again be traced when the groove depth is varied. They are localized in a layer a few wavelengths thick near the corrugated surface, as long as evanescent orders are responsible for their existence. The curls appear again on the line corresponding to $|\boldsymbol{P}| = 0$ for a plane surface. The primary differences when compared with the case of $d = 0.5$ μm (fig. 22) are, first, the curls are formed only in the near-field zone; going away from the grating they become increasingly smaller, and where the evanescent diffraction order vanish, the flow becomes the same as that above a flat surface. Second, the bottom curls are formed higher than the top curls, a direct consequence of which is that the direction of the energy flow for shallow gratings in the very near vicinity of the surface is opposite to that for the far-field flow. When h increases, the top curls unfold.

The increase of h moves the lowest bottom curls deeper into the grooves, and at a certain value of h they become totally hidden. This corresponds to zero phase difference between the waves reflected by the grating and the flat mirror. For this case the flow distribution above the grooves is identical to the flow above the flat surface, which can be expected considering the results for the grating supporting two diffraction orders.

An additional increase of the groove depth has the same effect on the energy flow distribution as it does for shallow gratings, except that inside each groove a curl goes increasingly deeper.

4.3. PLASMON SURFACE WAVE ALONG A METALLIC GRATING

Figures 23a and b represent the energy flow lines for two different values of groove depth: 0.058 and 0.395 μm, respectively. In these cases the surface wave propagating constant α^p have almost equal imaginary parts (fig. 16). The energy flow above the grooves is almost identical for the two gratings: near the surface the lines are almost parallel to it, corresponding to the physical fact that the surface wave propagates from left to right. Few lines end on the surface, leading to absorption losses. Some upper lines turn away from the surface, corresponding to radiation losses. As a result of both types of losses, the guided-wave amplitude decreases as it propagates along the grating, which is represented, in terms of the energy flow, as a decrease of the density of lines.

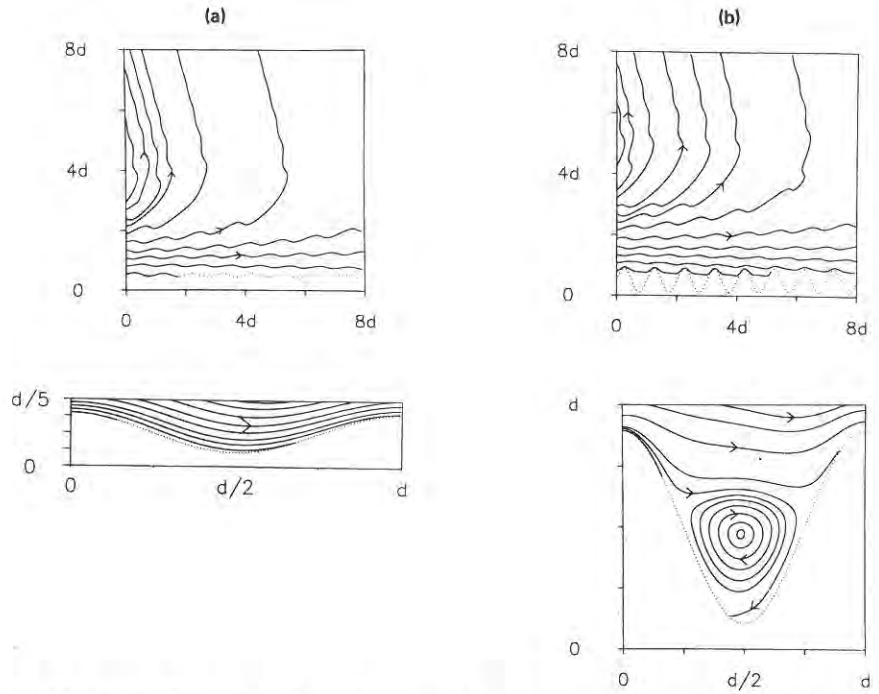

Fig. 23. Energy flow lines of a plasmon surface wave propagating along a shallow (a) $h = 0.058$ μm, and deep (b) $h = 0.395$ μm aluminum grating: $d = 0.5$ μm, $\lambda = 0.6328$ μm, TM polarization. (After Popov, Tsonev and Maystre [1990b].)

For a flat surface the energy flow direction is almost parallel to the surface (small losses). As h increases, the flow lines are pushed upwards by the groove tops, and above them the electromagnetic field power density increases. Inside the grooves the lines are thinned out, and the field density decreases. Nevertheless, the normalized average field density value over one period grows with h. The increase in the absorption losses is proportional to the increase of the average field density, and is almost an order greater than the growth of the absorbing surface area (fig. 8a). This is confirmed in the case of deep gratings: they can have lower absorption losses (e.g., $h/d = 0.72$), half those for a flat surface.

The primary difference between figs. 23a and b occurs inside the grooves: curls exist in each groove of a deep grating. Although some of the flow lines

reach the surface, closed curves in the deep grooves separate their bottoms from the energy flow above the tops, which explains why the absorption losses for deep gratings can take lower values than for shallow ones and even for a flat surface (fig. 8).

4.4. RESONANT TOTAL ABSORPTION OF LIGHT BY METALLIC GRATINGS

Total absorption of light by a metallic grating that accompanies surface wave excitation occurs for shallow, deep, and very deep grooves (fig. 11). Figure 24 shows the lines along which energy flows in the three different cases that

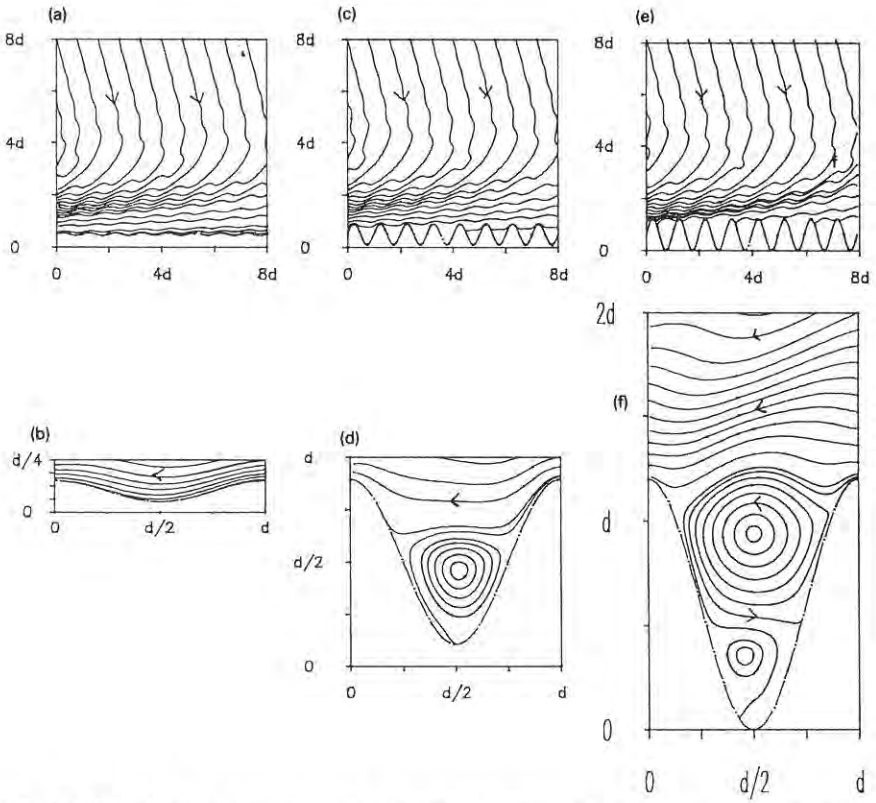

Fig. 24. Energy flow lines correspond to the total absorption of light by a sinusoidal aluminum grating: $d = 0.5$ μm, $\lambda = 0.6328$ μm, TM polarization. (a, b) $h = 0.05$ μm, (c, d) $h = 0.395$ μm, (e, f) $h = 0.6$ μm. (After Popov and Tsonev [1990].)

correspond to total absorption (i.e. matching the groove depth and angle of incidence for a given wavelength). Away from the grating surface (approximately above 10λ), the picture is equivalent to the far-zone energy flow distribution, i.e., the evanescent orders have no influence above a distance of 10λ. When total absorption of light occurs, the far zone is characterized by a uniform energy flow towards the grating that corresponds to the incident wave. As the surface is approached, the flow lines turn to the left and the line density increases. The near-zone energy flow distribution above the grooves represents a surface wave propagating to the left (the surface plasmon is excited through the first diffraction order). As can be expected, a close similarity is observed with fig. 23, except for the direction of the energy flow. The increase of the density of the flow lines leads to an enhancement of the electromagnetic field. This is usually expressed in terms of the ratio between the local optical power density

$$W = \varepsilon_0 n^2 |\boldsymbol{E}|^2 + \mu_0 |\boldsymbol{H}|^2 \tag{24}$$

and the power density of the incident wave (assumed to be equal to unity). As is usual, μ_0 stands for the vacuum permeability. For a flat surface, this ratio (later called "enhancement") does not exceed four. In the region of the resonant total absorption of light the enhancement can exceed several orders of magnitude. This phenomenon has been known in shallow gratings for a decade, and is believed to play a major role in the surface-enhanced Raman spectroscopy (SERS) and nonlinear excitation. Figure 25 shows the groove depth dependence of the field enhancement at the top and bottom of the grooves corres-

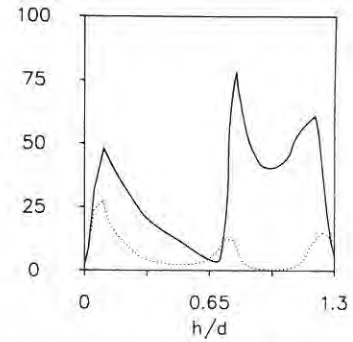

Fig. 25. Groove depth dependence of the normalized optical power density at the top (solid curve) and at the bottom (dotted curve) of the grooves of a sinusoidal aluminum grating: $d = 0.5$ μm, $\lambda = 0.6328$ μm, $\theta_0 = 14.93°$, TM polarization. (After Popov and Tsonev [1989].)

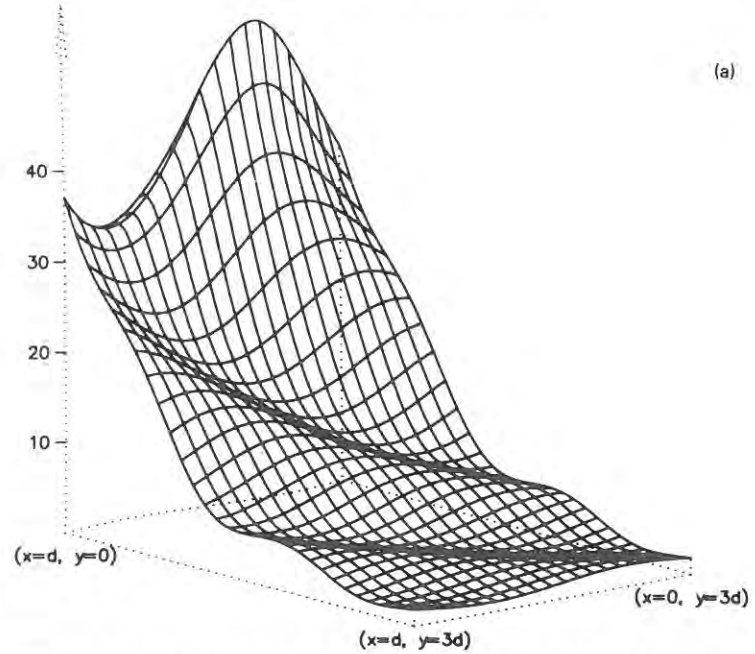

Fig. 26. 2D distribution of the electromagnetic power density in the vicinity of the grating surface, corresponding to the cases in fig. 24a, c, and e. (After Popov and Tsonev [1989].)

ponding to fig. 11. A 2D distribution of the optical power density near the grating surface is given in fig. 26 for the three cases of total light absorption. The primary difference in the values of the energy distribution is found inside the grooves. Whereas for shallow gratings the field enhancement at the top and bottom of the grooves is of an identical order (the difference does not exceed a factor of two; see, e.g., Garsia [1983a,b], Popov and Tsonev [1989]), in deep gratings the energy is localized at the tops of the groove. Phenomenologically, such an enhancement results from the existence of a pole of the scattering matrix. For the diffraction order that corresponds directly to the solution of the homogeneous problem (the first, in our case), the existence of a zero is unnecessary to compensate for the pole, since the plasmon surface wave with a propagation constant given by eq. (10) also exists for a flat surface. Thus, a substantial (resonant) increase of the amplitude of this particular order, described by eq. (15), could be expected. This phenomenon is illustrated in fig. 27 by the angular dependence of the first-order amplitude in the region of light absorption by shallow gratings. Moreover, since this order is evanescent far

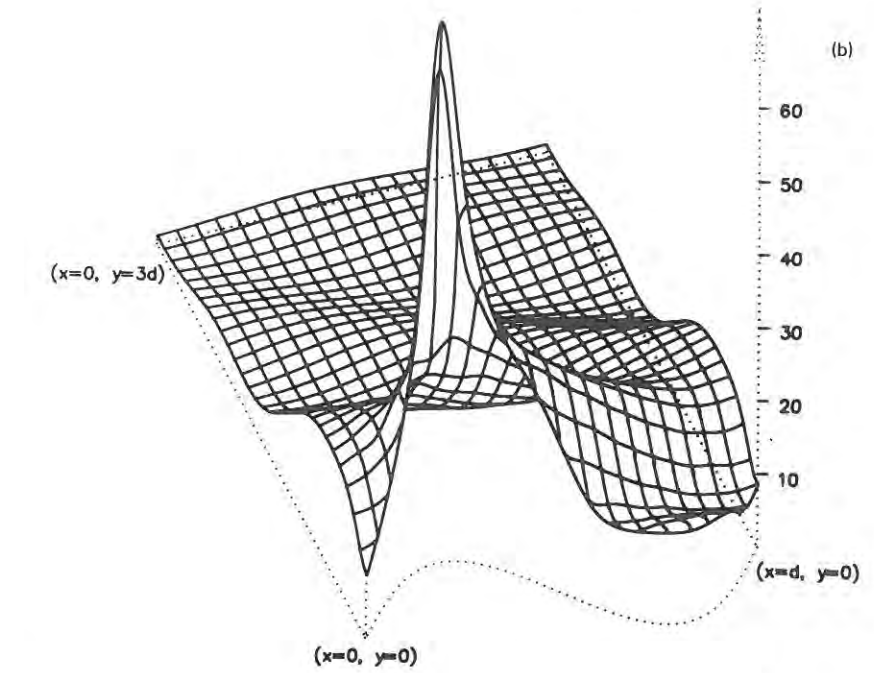

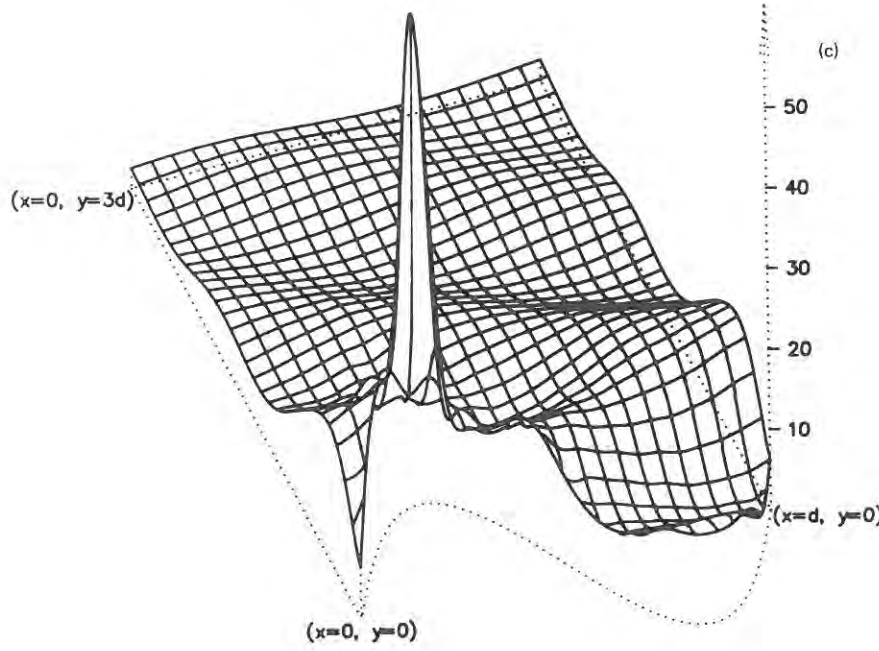

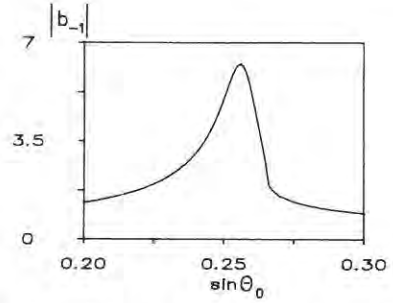

Fig. 27. The amplitude $|b_{-1}|$ of the first evanescent diffracted order as a function of α_0 in the vicinity of the total absorption of light by a shallow aluminum sinusoidal grating: $d = 0.5$ μm, $\lambda = 0.6328$ μm, $h = 0.05$ μm, TM polarization.

from the corrugated surface, the field enhancement is localized along the interface. However, the principal difference between fig. 26a on the one side and figs. 26b and c on the other can again be understood from the picture of the energy flow distribution (fig. 24), as follows.

Some lines very close to the surface turn downwards and finish at the metal surface. The energy flow through the grating boundary is exactly equal to the energy flow of the incident wave. By comparing figs. 24a, c and e, it can be observed that the energy flow distribution is almost identical above the top of the grooves for the total absorption of light in shallow, deep, and very deep gratings. Figures 24b, d and f show the peculiarities of each case. First, in shallow gratings ($h/d = 0.1$) the flow lines follow the grating surface. They are almost parallel to the metal–air boundary. Of course, some lines terminate at the surface, since the metal is not perfectly conducting. The line density above the top of the grooves is slightly greater than that above the bottom, since less space is present above the top than above the bottom. This results in a slight variation of the electromagnetic field enhancement values along the groove (fig. 25). Second, in deep gratings ($h/d = 0.79$ and $h/d = 1.2$) inside the grooves one or two curls are formed that separate the main energy flow from the bottom of the grooves. This separation is the reason why the electromagnetic field enhancement that accompanies the total absorption of light is exhibited at the tops but not at the bottoms of the deep grooves, in contrast with shallow gratings. Moreover, it should be remembered that in the middle of the curls in figs. 24d and f, $|\boldsymbol{P}| = W = 0$, whereas no such regions are observed in fig. 24b.

4.5. NONRESONANT TOTAL ABSORPTION OF LIGHT

Figures 28a and b correspond, respectively, to the energy flow distributions above and inside the grooves in the case of the nonresonant total absorption of light at grazing incidence (fig. 18 with $h/d = 0.69$, $\theta_0 = 87.86°$). It should be noted that this phenomenon is not strictly a total absorption of light: whereas the zeroth-order efficiency is exactly zero, the first-order efficiency is approximately 10^{-3}, but from a practical standpoint we can speak of the total absorption of light.

The energy flow distribution up to the close vicinity of the grating surface is almost the same as that in the far-field zone; no bending of the flow lines in the direction parallel to the surface is observed, in contrast with figs. 24a, c, and d, since no surface wave is excited in this case. As a result, no line density enlargement nor electromagnetic field enhancement appears. The total change of direction in fig. 28a in comparison with figs. 24a, c, and d is due to the difference in the angles of incidence. Inside the grooves (fig. 28b) the energy flow distribution is similar to that in fig. 24d; the groove depth values show little difference (in fig. 24d $h/d = 0.79$, and in fig. 28 $h/d = 0.69$). A curl is totally hidden inside each groove.

In the previous subsection a similarity exists between the pictures of the energy flow distribution above the grooves, but no similarity is observed inside them. When figs. 24 and 28 are compared, however, just the opposite occurs, i.e. the pictures inside the grooves are similar, but differ greatly above them.

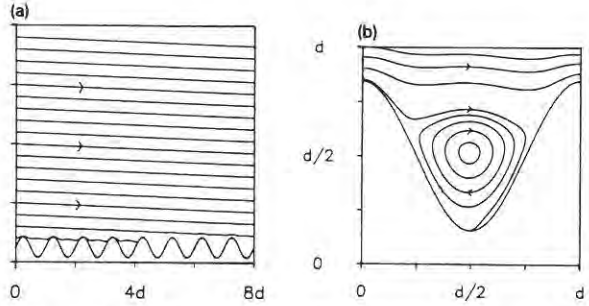

Fig. 28. Energy flow lines for the nonresonant total absorption of light, corresponding to the case in fig. 18a with $h = 0.345$ μm. (After Popov and Tsonev [1990].)

4.6. TOTAL INTERNAL REFLECTION BY DIELECTRIC GRATINGS

Perfect conductivity does not limit the generality of the results presented in §§ 4.1 and 4.2. Absorption losses cause some of the lowest flow lines to terminate on the surface, without modifying the flow distribution significantly. Moreover, similar flow distributions are obtained when a lossless dielectric grating is considered in the same mounting, supporting only two propagating reflected orders. Total internal reflection on a flat substrate–air boundary is characterized by an energy flow parallel to the interface. In air it has the same direction but with an exponentially decreasing amplitude. In the dielectric its horizontal component is equal to

$$P_x = \frac{\alpha_0}{\omega\mu_0} |E_z|^2 \tag{25a}$$

for TE polarization, and to

$$P_x = \frac{\alpha_0}{\omega\varepsilon_0 n^2} |H_z|^2 \tag{25b}$$

for TM polarization.

Similarly to the perfectly conducting case, the corrugation causes the flow lines to become curved and curls to be formed around the points where $|\boldsymbol{P}| = 0$. When the centers of the lowest curls are aligned with the tops of the grooves, perfect blazing occurs in the first order. There are, however, two important differences when compared with the metallic gratings.

(1) Both media are characterized by positive real values of the electric permittivity, and the energy flow can extend into the air. This fact has two direct consequences: (a) the lowest curls also spread in the second medium, and are larger in diameter than the corresponding curls for the metallic substrate; (b) at the bottom of the grooves, flow lines undulate along the corrugation and separate the bottoms from the lowest curls (fig. 29). Thus, deeper grooves are required to move the centers of the curls to the depth necessary to ensure any special phenomena, such as perfect blazing and antiblazing (compare figs. 5 and 13).

(2) Because of a partial penetration of the field inside the second medium even for a flat surface, the lines where $P_x = 0$ are given by more complex expressions than in eqs. (22). Their distance from the surface is determined by

$$\exp(-\mathrm{i}\chi_0^1 y_0) + \exp(\mathrm{i}\varphi)\exp(\mathrm{i}\chi_0^1 y_0) = 0\,, \tag{26}$$

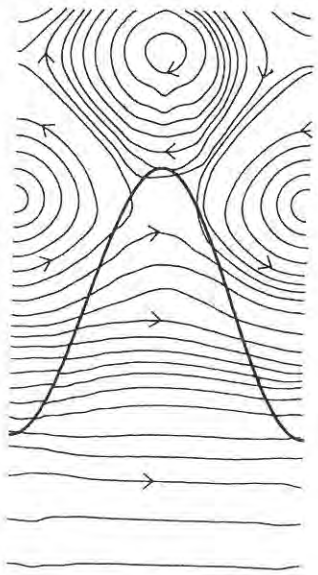

Fig. 29. Energy flow lines of the light diffracted by a dielectric grating in the total internal reflection regime: $n_1 = 1.5$, $n_2 = 1$, $\lambda = 0.55$ μm, $d = 0.26$ μm, $h = 0.24$ μm, TE polarization, and $\theta_0 = 45°$.

where the phase difference φ of the reflected light can be determined by Fresnel's formula, remembering that χ_0^2 is imaginary:

$$(b_0^1)_{\mathrm{TE}} \equiv \exp(\mathrm{i}\varphi_{\mathrm{TE}}) = \frac{1 - \chi_0^1/\chi_0^2}{1 + \chi_0^1/\chi_0^2}\,, \tag{27a}$$

$$(b_0^1)_{\mathrm{TM}} \equiv \exp(\mathrm{i}\varphi_{\mathrm{TM}}) = \frac{n_1^2 - \chi_0^1/\chi_0^2}{n_1^2 + \chi_0^1/\chi_0^2}\,. \tag{27b}$$

Taking into account the values of the system parameters in fig. 13, it directly follows that

$$y_0^{\mathrm{TM}} > y_0^{\mathrm{TE}}\,, \tag{28}$$

in contrast with the metallic substrate. Thus, perfect blazing for TM polarization is obtained for deeper grooves (fig. 13).

4.7. LIGHT REFRACTION BY DEEP TRANSMISSION GRATINGS

As mentioned in § 4.1, the process of curl formation can be explained by simply taking into account the interference between only *three* coherent waves. A reflection grating supporting two diffraction orders is the simplest model. Moreover, as discussed earlier, even a grating supporting a single order forms curls in the near-field zone, where evanescent orders are substantial. However, the mechanism of the diffraction of light by transmission gratings is entirely different. When a plane wave is incident on a flat interface between two lossless media, the flow lines are straight. In the upper medium their inclination depends on the angle of incidence and the surface reflectivity. In the lower medium, where only a single transmitted wave propagates, the energy flow follows the direction of the surface.

Corrugation does not lead to a substantial change in the distribution of

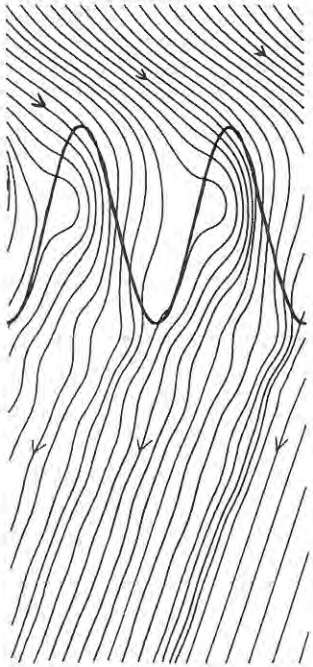

Fig. 30. Energy flow lines of the light diffracted by a transmission sinusoidal grating ($n_1 = 2.1$, $n_2 = 1$, $d = 0.4476\ \mu m$, $h = 0.6\ \mu m$, $\lambda = 0.6328\ \mu m$, TE polarization, and $\theta_0 = 45°$), having a 99% efficiency in the first transmitted order.

energy flow lines; inside the corrugated region the lines are slightly curved, depending on the amount of light diffracted in the non-zeroth transmitted orders. When almost the entire incident energy is diffracted into a single dispersive order, the energy flow in the lower medium follows its direction of propagation. This is the case with the grating, the efficiency behavior of which is shown in fig. 14. The flow distribution for the value of groove depth that ensures maximum efficiency in the first transmitted order is presented in fig. 30. It is surprising to discover that evanescent orders do not significantly modify the picture, providing only the smoothness of the curvature of lines inside the corrugated region.

Acknowledgements

The author is grateful to Dr. Erwin Loewen (Milton Roy Company, Rochester) for his major role in initiating and preparing this article.

References

Andrewartha, J. R., J. R. Fox and I. J. Wilson, 1979a, Opt. Acta **26**(1), 69.
Andrewartha, J. R., J. R. Fox and I. J. Wilson, 1979b, Opt. Acta **26**(2), 197.
Breidne, M., and D. Maystre, 1980, Periodic Structures, Gratings, Moiré Patterns and Diffraction Phenomena, Proc. SPIE **240**, 165.
Chandezon, J., M. Dupuis, G. Cornet and D. Maystre, 1981, J. Opt. Soc. Am. **72**, 839.
Chang, K. C., and T. Tamir, 1980, Appl. Opt. **19**, 282.
Chang, K. C., V. Shan and T. Tamir, 1980, J. Opt. Soc. Am. **70**, 804.
Coutaz, J. L., 1987, J. Opt. Soc. Am. B **4**, 105.
Coutaz, J. L., and R. Reinisch, 1985, Solid State Commun. **56**, 545.
Dumery, G., and P. Filippi, 1970, C. R. Hebd. Séances Acad. Sci. **270**, 137.
Enger, R. C., and S. K. Case, 1983, J. Opt. Soc. Am. **73**, 1113.
Fano, U., 1941, J. Opt. Soc. Am. **31**, 213.
Garsia, N., 1983a, Opt. Commun. **45**, 307.
Garsia, N., 1983b, J. Electron Spectrosc. Relat. Phenom. **29**, 421.
Hajnal, J. V., 1987, Proc. R. Soc. London A **414**, 447.
Hessel, A., and A. A. Oliner, 1965, Appl. Opt. **4**, 1275.
Hessel, A., J. Schmoys and D. Y. Tseng, 1975, J. Opt. Soc. Am. **65**, 380.
Hutley, M. C., 1982, Diffraction Gratings (Academic Press, New York).
Hutley, M. C., and D. Maystre, 1976, Opt. Commun. **19**, 431.
Loewen, E., 1983, Diffraction gratings, ruled and holographic, in: Appl. Opt. Opt. Eng., Vol. IX (Academic Press, New York) ch. 2.
Madden, R. P., and J. Strong, 1958, Diffraction gratings, in: Concepts of Classical Optics, ed. J. Strong (Freeman, San Francisco, CA).
Mashev, L., and E. Loewen, 1988, Appl. Opt. **27**, 31.
Mashev, L., and E. Popov, 1984, Opt. Commun. **51**, 131.

Mashev, L., and E. Popov, 1989, J. Opt. Soc. Am. **6**, 1561.
Mashev, L., E. Popov and E. Loewen, 1988, Appl. Opt. **27**, 152.
Mashev, L., E. Popov and E. Loewen, 1989, Appl. Opt. **28**, 2538.
Mashev, L., E. Popov and D. Maystre, 1988, Opt. Commun. **67**, 321.
Maystre, D., 1972, Opt. Commun. **6**, 50.
Maystre, D., 1973, Opt. Commun. **8**, 216.
Maystre, D., 1978a, J. Opt. Soc. Am. **68**, 490.
Maystre, D., 1978b, Opt. Commun. **26**, 127.
Maystre, D., 1980, Integral methods, in: Electromagnetic Theory of Gratings, ed. R. Petit (Springer, Berlin) ch. 3.
Maystre, D., 1982, General study of grating anomalies from electromagnetic surface modes, in: Electromagnetic Surface Modes, ed. A. D. Boardman (Wiley, New York) ch. 17.
Maystre, D., 1984a, Rigorous vector theories of diffraction gratings, in: Progress in Optics, Vol. XXI, ed. E. Wolf (North-Holland, Amsterdam) ch. 1.
Maystre, D., 1984b, J. Opt. (France) **15**, 43.
Maystre, D., and M. Cadilhac, 1981, Radio Sci. **16**, 1003.
Maystre, D., and M. Neviere, 1977, J. Opt. (France) **8**, 165.
Maystre, D., and R. Petit, 1976, Opt. Commun. **17**, 196.
Maystre, D., M. Cadilhac and J. Chandezon, 1981, Opt. Acta **28**, 457.
Maystre, D., J. P. Laude, P. Gacoin, D. Lepere and J. P. Priou, 1980, Appl. Opt. **19**, 3099.
Maystre, D., M. Neviere and P. Vincent, 1978, Opt. Acta **25**, 905.
Maystre, D., M. Neviere, R. Reinisch and J. L. Coutaz, 1988, J. Opt. Soc. Am. B **5**, 338.
McClellan, R. P., and G. W. Stroke, 1966, J. Math. Phys. **45**, 383.
McPhedran, R. C., and D. Maystre, 1974, Nouv. Rev. Opt. **5**, 241.
Mermit, N. D., 1990, Phys. Today **11**, 9.
Metcalfe, K., and R. Hester, 1983, Chem. Phys. Lett. **94**, 411.
Millar, R. F., 1961a, Can. J. Phys. **39**, 81.
Millar, R. F., 1961b, Can. J. Phys. **39**, 104.
Millar, R. F., 1971a, Proc. Cambridge Philos. Soc. **69**, 175.
Millar, R. F., 1971b, Proc. Cambridge Philos. Soc. **69**, 217.
Moaveni, M. K., H. A. Kalhor and A. Afrashteh, 1975, Comput. Electron. Eng. **2**, 265.
Moharam, M. G., and T. K. Gaylord, 1982, J. Opt. Soc. Am. **72**, 1385.
Moharam, M. G., T. K. Gaylord, G. T. Sincerbox, H. Werlich and B. Yung, 1984, Appl. Opt. **23**, 3214.
Neureuther, A., and K. Zaki, 1969, URSI Symp. Electron. Waves, Alta Freq. **38**, 282.
Neviere, M., 1980, The homogeneous problem, in: Electromagnetic Theory of Gratings, ed. R. Petit (Springer, Berlin) ch. 5.
Neviere, M., and M. Cadilhac, 1970, Opt. Commun. **2**, 235.
Neviere, M., and R. Reinisch, 1983, J. Phys. Colloq. (Paris) **44**, Suppl. 12, C10-359.
Neviere, M., H. Akhouayri, P. Vincent and R. Reinisch, 1987, Proc. Soc. Photo-Opt. Instrum. Eng. **815**, 146.
Neviere, M., M. Cadilhac and R. Petit, 1972, Opt. Commun. **6**, 34.
Neviere, M., M. Cadilhac and R. Petit, 1973, IEEE Trans. Antennas Propag. **AP-21**, 37.
Neviere, M., P. Vincent and R. Petit, 1974, Nouv. Rev. Opt. **5**, 65.
Pavageau, J., R. Eido and H. Kobeisse, 1967, C. R. Hebd. Séances Acad. Sci. B **264**, 424.
Petit, R., 1966a, Rev. Opt. **45**, 249.
Petit, R., 1966b, Rev. Opt. **45**, 353.
Petit, R., ed., 1980, Electromagnetic Theory of Gratings (Springer, Berlin).
Petit, R., and M. Cadilhac, 1964, C. R. Hebd. Séances Acad. Sci. B **259**, 2077.
Petit, R., and M. Cadilhac, 1966, C. R. Hebd. Séances Acad. Sci. B **262**, 468.
Petit, R., and M. Cadilhac, 1987, Radio Sci. **22**, 1247.

Popov, E., 1989, J. Mod. Opt. **36**, 669.
Popov, E., and L. Tsonev, 1989, Opt. Commun. **69**, 193.
Popov, E., and L. Tsonev, 1990, Surf. Sci. **230**, 290.
Popov, E., L. Mashev and E. Loewen, 1989, Appl. Opt. **28**, 970.
Popov, E., L. Mashev and D. Maystre, 1986, Opt. Acta **33**, 607.
Popov, E., L. Mashev and D. Maystre, 1988, Opt. Commun. **65**, 97.
Popov, E., L. Tsonev and D. Maystre, 1990a, J. Mod. Opt. **37**, 367.
Popov, E., L. Tsonev and D. Maystre, 1990b, J. Mod. Opt. **37**, 379.
Rayleigh, Lord, 1907, Proc. R. Soc. London A **79**, 399.
Reinisch, R., and M. Neviere, 1981, Opt. Eng. **20**, 629.
Reinisch, R., G. Chartier, M. Neviere, M. C. Hutley, G. Clauss, J. P. Galaup and J. F. Eloy, 1983, J. Phys. (Paris) Lett. **44**, L1007.
Roumiguieres, J. L., D. Maystre and R. Petit, 1976, J. Opt. Soc. Am. **66**, 772.
Tseng, D. Y., A. Hessel and A. A. Oliner, 1969, URSI Symp. Electron. Waves, Alta Freq., special issue **38**, 82.
Twersky, V., 1956, IRE Trans. Antennas Propag. **AP-4**, 330.
Twersky, V., 1960, J. Res. Nat. Bur. Stand. D **64**, 715.
Uretsky, J. L., 1965, Ann. Phys. (New York) **33**, 400.
Van den Berg, P. M., 1971, Appl. Sci. Res. **24**, 261.
Van den Berg, P. M., 1981, J. Opt. Soc. Am. **71**, 1224.
Van den Berg, P. M., and J. T. Fokkema, 1979, J. Opt. Soc. Am. **69**, 27.
Vincent, P., 1980, Differential methods, in: Electromagnetic Theory of Gratings, ed. R. Petit (Springer, Berlin) ch. 4.
Wirgin, A., 1964, Rev. Opt. **43**, 499.
Wirgin, A., 1968, Rev. Cethedec **5**, 131.
Wirgin, A., 1979a, C. R. Hebd. Séances Acad. Sci. A **289**, 259.
Wirgin, A., 1979b, C. R. Hebd. Séances Acad. Sci. B **288**, 179.
Wirgin, A., 1979c, C. R. Hebd. Séances Acad. Sci. B **289**, 273.
Wirgin, A., 1980, Opt. Acta **27**, 1671.
Wirgin, A., 1981, Opt. Acta **28**, 1377.
Wood, R. W., 1902, Philos. Mag. **4**, 396.
Yamashita, M., and M. Tsuji, 1983, J. Phys. Soc. Jpn. **52**, 2462.
Yokomori, K., 1984, Appl. Opt. **23**, 2303.